1 **A transient role of primary cilia in controlling direct versus indirect neurogenesis in the**

2 **developing cerebral cortex**

3

4 Kerstin Hasenpusch-Theil[1], Christine Laclef[2,3], Matt Colligan[1], Eamon Fitzgerald[1], Katherine

5 Howe[1], Emily Carroll[1], Shaun R. Abrams[4], Jeremy F. Reiter[4,5], Sylvie Schneider-Maunoury[2], and

6 Thomas Theil[1,6]

7

8

9

10 [1]Centre for Discovery Brain Sciences, Hugh Robson Building, University of Edinburgh, Edinburgh,

11 EH8 9XD, United Kingdom

12 [2] Sorbonne Université, CNRS UMR7622, INSERM U1156, Institut de Biologie Paris Seine (IBPS) -

13 Developmental Biology Unit, 75005, Paris, France

14 [3]Present address: Sorbonne Université, Institut du Fer à Moulin INSERM U1270, Paris, France

15 [4]Department of Biochemistry and Biophysics, University of California, San Francisco, CA 94143

16 [5]Chan Zuckerberg Biohub, San Francisco, CA94158, USA Chan Zuckerberg Biohub, San

17 Francisco, CA 94158, USA

18 [6]Author for correspondence (email: thomas.theil@ed.ac.uk)

19

20

21 **Running title:** Inpp5e and direct/indirect neurogenesis

22

23 **Key words:** *Inpp5e*; *Tctn2*; primary cilia; neurogenesis; cortex

24

25

26

27

28 **ABSTRACT**

29

30 During the development of the cerebral cortex, neurons are generated directly from radial glial cells

31 or indirectly via basal progenitors. The balance between these division modes determines the

32 number and types of neurons formed in the cortex thereby affecting cortical functioning. Here, we

33 investigate the role of primary cilia in this process. We show that a mutation in the ciliary gene *Inpp5e*

34 leads to a transient increase in direct neurogenesis and subsequently to an overproduction of layer

35 V neurons in newborn mice. Loss of *Inpp5e* also affects ciliary structure coinciding with increased

36 Akt and mTOR signalling and reduced Gli3 repressor levels. Genetically re-storing Gli3 repressor

37 rescues the decreased indirect neurogenesis in *Inpp5e* mutants. Overall, our analyses reveal how

38 primary cilia determine neuronal subtype composition of the cortex by controlling direct vs indirect

39 neurogenesis. These findings have implications for understanding cortical malformations in

40 ciliopathies with *INPP5E* mutations.

41

INTRODUCTION

Building a functional cerebral cortex which confers humans with their unique cognitive capabilities requires controlling the proliferation of neural progenitor cells and the timing and modes of neurogenic cell divisions. Varying the timing and modes of neurogenesis affects neuronal numbers and subtype composition of the cortex (Florio & Huttner, 2014). In the developing murine cortex, radial glial cells (RGCs) represent the major neural stem cell type. Residing in the ventricular zone, they express Pax6 and undergo interkinetic nuclear migration dividing at the ventricular surface (Götz, Stoykova, & Gruss, 1998; Warren et al., 1999). Initially, RGCs go through rounds of symmetric proliferative divisions to produce two RGCs increasing the progenitor pool but switch to asymmetric divisions at the beginning of cortical neurogenesis. RGCs generate neurons in two ways, either directly or indirectly via the production of basal progenitors (BPs) that settle in the subventricular zone (SVZ) and express the Tbr2 transcription factor (Englund et al., 2005). In the mouse, the majority of BPs divide once to produce two neurons whereas the remainders undergo one additional round of symmetric proliferative division before differentiating into two neurons (Haubensak, Attardo, Denk, & Huttner, 2004; Miyata et al., 2004; Noctor, Martinez-Cerdeno, Ivic, & Kriegstein, 2004). In this way, BPs increase neuron output per radial glial cell and have therefore been implicated in the evolutionary expansion of the mammalian cerebral cortex (Martinez-Cerdeno, Noctor, & Kriegstein, 2006). Thus, the balance between direct and indirect neurogenesis is an important factor in generating appropriate neuron numbers and types.

The mechanisms that fine tune this balance and thereby adjust the numbers and types of neurons produced in the cortex have only recently been investigated. Mitotic spindle orientation (Postiglione et al., 2011) and endoplasmic reticulum (ER) stress (Gladwyn-Ng et al., 2018; Laguesse et al., 2015) are contributing factors to control the generation of basal progenitors. In addition, levels of Slit/Robo and Notch/Delta signaling were shown to be evolutionarily conserved factors that determine the predominant mode of neurogenesis (Cardenas et al., 2018). Moreover, feedback signals from postmitotic neurons control the fate of radial glial daughter cells involving the release of Neurotrophin-3 and Fgf9 (Parthasarathy, Srivatsa, Nityanandam, & Tarabykin, 2014; Seuntjens et al., 2009) as well as the activation of a Notch-dependent signaling pathway (W. Wang et al., 2016). These studies highlight the importance of cell-cell signaling in controlling the cell lineage of cortical progenitors (Silva, Peyre, & Nguyen, 2019) and emphasize the necessity of studying the cellular mechanisms by which these signals control the decision by RGCs to undergo direct or indirect neurogenesis.

Given the importance of cell-cell signaling, it is likely that the primary cilium, a signaling hub in embryogenesis in general and in neural development in particular (Valente, Rosti, Gibbs, & Gleeson, 2014), plays key roles in determining the balance between direct versus indirect neurogenesis. The cilium is a subcellular protrusion that predominately emanates from the apical surface of radial glial cells projecting into the ventricular lumen. The phenotypes of several mouse

80   lines mutant for ciliary genes underline the importance of the primary cilium in forebrain development
81   but these mutants often suffer from severe patterning defects (Ashique et al., 2009; Besse et al.,
82   2011; Willaredt et al., 2008) which make studying ciliary roles in determining the lineage of cortical
83   progenitors difficult. To address such functions, we investigated corticogenesis in a mouse mutant
84   for the ciliary gene *Inpp5e*.

85   *INPP5E* is mutated in Joubert syndrome (JS) (Bielas et al., 2009; Jacoby et al., 2009), a
86   ciliopathy characterized by cerebellar defects in which a subset of patients also shows malformations
87   of the cerebral cortex including heterotopias, polymicrogyria and agenesis of the corpus callosum
88   (Valente et al., 2014). *Inpp5e* encodes Inositol polyphosphate 5 phosphatase E, an enzyme that is
89   localized in the ciliary membrane and that hydrolyses the phosphatidylinositol polyphosphates
90    $PI(4,5)P_2$ and $PI(3,4,5)P_3$ (Bielas et al., 2009; Jacoby et al., 2009). In this way, it controls the inositol
91   phosphate composition of the ciliary membrane and thereby regulates the activity of several
92   signaling pathways and cilia stability (Bielas et al., 2009; Chavez et al., 2015; Garcia-Gonzalo et al.,
93   2015; Jacoby et al., 2009; Plotnikova et al., 2015). In contrast to *Inpp5e*'s extensively studied
94   biochemical and cellular roles, little is known how these diverse functions are employed at the tissue
95   level to control RGC lineage.

96   Here, we show that loss of *Inpp5e* function results in an increase in neuron formation at the
97   expense of basal progenitor production in the E12.5 cortex and in an overproduction of Ctip2+ layer
98   V neurons in newborn mutants. Moreover, RGC cilia show unusual membranous structures and/or
99   abnormal numbers of microtubule doublets affecting the signaling capabilities of the cilium. The
100   levels of Gli3 repressor (Gli3R), a critical regulator of cortical stem cell development (Hasenpusch-
101   Theil et al., 2018; H. Wang, Ge, Uchida, Luu, & Ahn, 2011), is reduced and re-introducing Gli3R
102   rescues the decreased formation of basal progenitors. Taken together, these findings implicate the
103   primary cilium in controlling the decision of RGCs to either undergo direct neurogenesis or to form
104   basal progenitors, thereby governing the neuronal subtype composition of the cerebral cortex.

105

106   **RESULTS**

107

108   ***Inpp5e^{Δ/Δ}* embryos show mild telencephalic patterning defects**

109   Controlling the balance between direct and indirect neurogenesis in the developing cerebral

110   cortex is mediated by cell-cell signaling (Cardenas et al., 2018) and is hence likely to involve the

111   primary cilium. To investigate potential ciliary roles, we started characterizing cortical stem cell

112   development in embryos mutant for the *Inpp5e* gene which has a prominent role in ciliary signaling

113   and stability. Mutations in ciliary genes have previously been found to result in telencephalon

114   patterning defects, most notably in a ventralisation of the dorsal telencephalon and/or in defects at

115   the corticoseptal (CSB) and pallial/subpallial boundaries (PSPB) (Ashique et al., 2009; Besse et al.,

116   2011; Willaredt et al., 2008). Therefore, we first considered the possibility that such early patterning

117   defects may be present in *Inpp5e* mutant embryos and could affect cortical stem cell development.

118   In situ hybridization and immunofluorescence analyses of E12.5 control and *Inpp5e^{Δ/Δ}* embryos

119   revealed no obvious effect on the expression of dorsal and ventral telencephalic markers at the

120   corticoseptal boundary (SupFig. 1). In contrast, the pallial/subpallial boundary was not well defined

121   with a few scattered Pax6+ and *Dlx2* expressing cells on the wrong side of the boundary, i.e. in the

122   subpallium and pallium, respectively (SupFig. 1). Moreover, the hippocampal anlage appeared

123   smaller and disorganized with low level and diffuse expression of cortical hem markers (SupFig. 2),

124   consistent with known roles of Wnt/β-catenin and Bmp signaling in hippocampal development

125   (Galceran, Miyashita-Lin, Devaney, Rubenstein, & Grosschedl, 2000; Lee, Tole, Grove, & McMahon,

126   2000). In contrast, progenitors in the neocortical ventricular zone of *Inpp5e* mutant mice expressed

127   the progenitor markers *Emx1*, *Lhx2*, *Pax6* and *Ngn2,* though the levels of Pax6 protein expression

128   appeared reduced in the medial neocortex suggestive of a steeper lateral to medial Pax6 expression

129   gradient in mutant embryos. These expression patterns were maintained in E14.5 *Inpp5e^{Δ/Δ}* embryos

130   but revealed an area in the very caudal/dorsal telencephalon where the neocortex was folded

131   (SupFig. 3). At this level, folds were also present in the hippocampal anlage. Taken together, these

132   findings indicate that *Inpp5e* mutants have mild patterning defects affecting the integrity of the PSPB,

133   hippocampal development and the caudal-most neocortex while the rostral neocortex shows no

134   obvious malformation and can therefore be analysed for effects of the *Inpp5e* mutation on direct and

135   indirect neurogenesis.

136

137   ***Inpp5e* controls direct vs indirect neurogenesis in the lateral neocortex**

138   Based upon these findings, we started analyzing the proliferation and differentiation of radial

139   glial cells in *Inpp5e^{Δ/Δ}* embryos in the rostrolateral and rostromedial neocortex to avoid the

140   regionalization defects described above. As a first step, we determined the proportion of radial glial

141   cells, basal progenitors and neurons in these regions in E12.5 embryos. Double

142   immunofluorescence for PCNA which labels all progenitor cells (Hall et al., 1990) and the radial glial

5

143 marker Pax6 did not reveal differences in the proportions of radial glial cells at both medial and lateral

144 levels (Fig. 1A-D). In contrast, the proportion of Tbr2+ basal progenitors was reduced laterally but

145 not medially (Fig. 1E-H). This decrease coincided with an increase in Tbr1+ neurons specifically in

146 the lateral neocortex (Fig. 1I-L). To determine whether these alterations are maintained at a later

147 developmental stage, we repeated this investigation in E14.5 embryos. This analysis revealed no

148 significant differences in the proportion of Pax6+ RGCs (Fig. 2A-D). Similarly, there was no alteration

149 in the proportion of Tbr2+ basal progenitors in lateral neocortex, however, their proportion was

150 reduced medially (Fig. 2E-H).

151   To label cortical projection neurons, we used double immunofluorescence for Tbr1 and Ctip2

152 which allowed us to distinguish between Ctip2+Tbr1+ and Ctip2+Tbr1- neurons. Quantifying these

153 subpopulations showed no effect on the formation of Ctip2+Tbr1+ neurons in $Inpp5e^{\Delta/\Delta}$ embryos. In

154 contrast, the proportion of Ctip2+Tbr1- neurons was reduced medially but increased in the lateral

155 neocortex (Fig. 2I-R). Taken together, these findings show that initially Tbr1+ and later Ctip2+Tbr1-

156 neurons were increasingly formed in the lateral neocortex of $Inpp5e^{\Delta/\Delta}$ embryos and that the

157 proportion of basal progenitors recovered after an initial down-regulation.

158   To address the defective cellular processes underlying these neurogenesis defects in $Inpp5e$

159 mutants, we first measured proliferation rates of cortical progenitors and performed double

160 immunofluorescence for PCNA and pHH3 which labels mitotic radial glial cells located at the

161 ventricular surface and dividing basal progenitors in abventricular positions (SupFig. 4). This analysis

162 revealed no statistically significant differences in the E12.5 and E14.5 lateral neocortex of control

163 and $Inpp5e^{\Delta/\Delta}$ embryos. The proportion of mitotic basal progenitors, however, was reduced in the

164 E12.5 medial neocortex (SupFig. 4).

165   The cell cycle represents another key regulator of neuronal differentiation and a mutation in

166 $Kif3a$ affects ciliogenesis and the cell cycle in the developing neocortex (Wilson, Wilson, Wang,

167 Wang, & McConnell, 2012). To investigate the possibility of altered cell cycle kinetics, we used a

168 BrdU/IdU double labelling strategy (Martynoga, Morrison, Price, & Mason, 2005; Nowakowski,

169 Lewin, & Miller, 1989) to determine S phase length and total cell cycle length in radial glial cells and

170 found no statistically significant changes in these parameters (SupFig. 5).

171   Finally, the increased neuron production could also be explained by an increase in direct

172 neurogenesis at the expense of basal progenitor cell formation. To test this possibility, we gave BrdU

173 to E11.5 pregnant mice 24h before dissecting the embryos. We then used BrdU immunostaining in

174 conjunction with Tbr1 and Tbr2 to identify the neurons and basal progenitors formed in the lateral

175 neocortex within the 24h time period. This analysis showed that the proportion of Tbr1+ neurons

176 compared to the total number of BrdU+ cells increased while the Tbr2+ proportion decreased in

177 $Inpp5e$ mutants (Fig. 3). Since the cell cycle of basal progenitors is longer than 24h (Arai et al.,

178 2011), the 24h interval used in our cell cycle exit experiment was too short for newly formed basal

179 progenitors to undergo one additional round of the cell cycle and as the BrdU label would have been

180   diluted with a further round of division, this analysis supports our hypothesis that direct neurogenesis

181   became more prevalent in *Inpp5e*$^{\Delta/\Delta}$ radial glial cells.

182

183   **Cortical malformations in *Inpp5e*$^{\Delta/\Delta}$ embryos**

184   Next, we investigated the consequences of this increase in direct neurogenesis on cortical

185   size and layer formation. Since *Inpp5e*$^{\Delta/\Delta}$ newborn pups die perinatally (Bielas et al., 2009), we

186   focused our analysis on E18.5 embryos. The mutant lacked obvious olfactory bulbs, as revealed by

187   whole mounts of control and mutant brains (SupFig. 6). To gain insights into the overall histology of

188   the mutant forebrain, we stained coronal sections with DAPI. This analysis showed that the mutant

189   cortex was thinner laterally but not medially with a more pronounced reduction of the thickness at

190   caudal levels (SupFig. 7). In addition, the hippocampus was malformed with a smaller dentate gyrus.

191   Investigating the expression of markers characteristic of the entire hippocampus (*Nrp2*; (Galceran

192   et al., 2000)), the CA1 field (Scip1; (Frantz, Bohner, Akers, & McConnell, 1994)) and the dentate

193   gyrus (Prox1; (Oliver et al., 1993)) showed that these hippocampal structures were present but were

194   severely reduced in size and disorganized in *Inpp5e*$^{\Delta/\Delta}$ embryos (SupFig. 8). In addition, the corpus

195   callosum, the major axon tract connecting the two cerebral hemispheres, was correctly formed but

196   was smaller. We confirmed this effect by staining callosal axons and surrounding glial cells that guide

197   these axons to the contralateral hemisphere with L1 and GFAP, respectively (SupFig. 9).

198   After characterizing the gross morphology of the *Inpp5e*$^{\Delta/\Delta}$ cortex, we next investigated

199   whether the increased neuron formation in E12.5 mutant embryos led to changes in the neuronal

200   subtype composition of the E18.5 cortex. To this end, we used immunofluorescence labelling for

201   Tbr1 and Ctip2 to analyse the formation of layer VI and V neurons, respectively, whereas Satb2

202   served as a layer II-IV marker (Fig. 4). Inspecting these immunostainings at low magnification

203   showed that Tbr1+, Ctip2+ and Satb2+ neurons occupied their correct relative laminar positions in

204   *Inpp5e* mutants (Fig. 4A-F) except for neuronal heterotopias which were present in all mutant brains,

205   though their number and position varied (Fig. 4D). These immunostainings also revealed a medial

206   shift in the position of the rhinal fissure, a sulcus that is conserved across mammalian species and

207   separates neocortex from the paleocortical piriform cortex (Ariens-Kapers, Huber, & Crosby, 1936).

208   This shift was more marked caudally and suggests a dramatic expansion of the *Inpp5e* mutant

209   piriform cortex at the expense of neocortex at caudal most levels (Fig. 4D-F). Using the Tbr1/Ctip2

210   and Satb2 stainings, we determined the proportions of deep and superficial layer neurons,

211   respectively. Because of the expanded piriform cortex in *Inpp5e* mutants, we limited this

212   investigation to the unaffected rostral neocortex. In the rostrolateral neocortex, we found the

213   proportion of Tbr1+ neurons to be reduced (Fig. 4G, H, M). This reduction coincided with an

214   increased proportion of Ctip2+ layer V neurons (Fig. 4I, J, N) while the Satb2 population was

215   unchanged (Fig. 4K, L, O). In contrast, the rostromedial neocortex did not show any differences (Fig.

216   4P-X). Thus, the increase in direct neurogenesis in the lateral neocortex during earlier development

217   concurs with a change in the proportions of E18.5 Tbr1+ and Ctip2+ deep layer neurons.

218

219   **A mutation in the ciliary gene *Tctn2* leads to increased telencephalic neurogenesis**

220   To start to unravel the mechanisms by which *Inpp5e* controls cortical stem cell development,

221   we first analysed whether the increased early neurogenesis is restricted to *Inpp5e*$^{\Delta/\Delta}$ mutants or is

222   observed in another mutant affecting cilia. To this end, we focused on the *TECTONIC 2* (*TCTN2*)

223   gene which is crucial for ciliary transition zone architecture (Shi et al., 2017) and which, like *INPP5E*,

224   is mutated in Joubert Syndrome (Garcia-Gonzalo et al., 2011). Interestingly, E12.5 *Tctn2*$^{-/-}$ mutant

225   embryos (Reiter & Skarnes, 2006) also showed an increased proportion of Tbr1+ projection neurons

226   and a concomitant decrease in Tbr2+ basal progenitors in the dorsolateral telencephalon (Fig. 5).

227   Due to embryonic lethality, however, we were not able to investigate the formation of cortical neurons

228   at later stages.

229

230   **Ciliary defects in the forebrain of E12.5 *Inpp5e*$^{\Delta/\Delta}$ embryos**

231   Our findings in the *Inpp5e* and *Tctn2* mutants suggested a role for cilia in cortical progenitor

232   cells to control early neurogenesis. Therefore, we examined the presence and the structure of

233   primary cilia in the developing forebrain of *Inpp5e*$^{\Delta/\Delta}$ embryos by immunofluorescence and electron

234   microscopy. We first analyzed the presence of the small GTPase Arl13b, enriched in ciliary

235   membranes, and of γ-Tubulin (γTub), a component of basal bodies (Caspary, Larkins, & Anderson,

236   2007). We found no major difference in the number, the apical localization or the size of cilia in

237   control and *Inpp5e*$^{\Delta/\Delta}$ neuroepithelial cells in the E12.5 telencephalon (Fig. 6A,B) or diencephalon

238   (data not shown).

239   To gain insights into the fine structure of these primary cilia we performed electron

240   microscopy analyses. Scanning electron microscopy (SEM) provided an observation of the cilia

241   protruding into the telencephalic ventricles. In control embryos, almost all radial glial cells had a

242   single, ~1 μm long primary cilium (Fig. 6C), as previously described (Besse et al., 2011). Some

243   *Inpp5e*$^{\Delta/\Delta}$ mutant cells also displayed an apparently normal cilium (Fig. 6D, E), whereas other cells

244   harbored abnormal cilia, either with a lateral blob (arrowhead in Fig. 6D) or as a short and bloated

245   cilium-like protrusion (arrows in Fig. 6D,E).

246   Transmission electron microscopy (TEM) confirmed the presence of abnormal cilia in

247   *Inpp5e*$^{\Delta/\Delta}$ embryos. Cilia were recognized by basal bodies anchored to the apical membrane in both

248   control and *Inpp5e*$^{\Delta/\Delta}$ radial glial cells (Fig. 6F-L, N, Q). However, in *Inpp5e*$^{\Delta/\Delta}$ cells, some cilia lacked

249   the axoneme and showed unusual membranous structures that resemble budding vesicles emerging

250   from the lateral surface of the cilium (Fig. 6G, K), internal vesicles (arrows in Fig. 6I, K, L), or

251   undulating peripheral membranes (Fig. 6I), indicating an *Inpp5e*-dependent defect in ciliary

252   membrane morphology. Transverse sections revealed the presence of cilia with apparently normal

253 9+0 axonemes, as well as cilia containing abnormal numbers of microtubule doublets in *Inpp5e*$^{\Delta/\Delta}$

254 embryos (Fig. 6O, P). To quantify these ciliary defects, we counted the number of normal versus

255 abnormal cilia on TEM images obtained from control and *Inpp5e*$^{\Delta/\Delta}$ embryos, and found an increase

256 in abnormal cilia in *Inpp5e*$^{\Delta/\Delta}$ compared to control embryos (Fig. 6R). Taken together, a significant

257 number of abnormal primary cilia were found at the apical end of E12.5 radial glial cells in the

258 forebrain of *Inpp5e*$^{\Delta/\Delta}$ embryos. These abnormalities are consistent with a role of *Inpp5e* in

259 maintaining cilia stability (Jacoby et al., 2009).

260

261 **Receptor tyrosine kinase and mTOR signaling in *Inpp5e*$^{\Delta/\Delta}$ embryos**

262 Given these defects in ciliary structure, we started to investigate cilia-controlled signaling

263 pathways, defects in which might underlie the increased direct neurogenesis in the *Inpp5e*$^{\Delta/\Delta}$ mutant

264 radial glial cells. Inpp5e hydrolyzes the 5-phosphate of PI(3,4,5)P$_3$ which serves as a second

265 messenger in receptor tyrosine kinase signaling. We therefore investigated the amount and

266 distribution of pErk1/2 as a read-out of receptor tyrosine kinase signaling. Western blots using

267 dissected dorsal telencephalon from E12.5 and E14.5 embryos revealed no difference in the ratio

268 between pErk1/2 and Erk1/2 (SupFig. 10). Moreover, pErk1/2 expression in the E12.5 forebrain

269 remains restricted to the LGE, the diencephalon and to meninges covering the telencephalon but

270 was not identified in cortical progenitors (SupFig. 10). In E14.5 embryos, we detected pErk1/2

271 immunoreactivity in cortical progenitors in a lateral to medial gradient covering the whole extent of

272 the neocortex. In contrast, high level pErk1/2 expression remained confined to the lateral neocortex

273 with little or no expression medially in *Inpp5e*$^{\Delta/\Delta}$ embryos (SupFig. 10). These findings suggest that

274 pErk signaling does not play a role in the early neurogenesis defect in *Inpp5e* mutants but may be

275 involved in the recovery of basal progenitor formation.

276 PI(3,4,5)P$_3$, a substrate of the Inpp5e phosphatase, is essential for the effective activation of

277 the serine threonine kinase Akt (Kisseleva, Cao, & Majerus, 2002; Plotnikova et al., 2015) raising

278 the possibility that loss of *Inpp5e* results in activated Akt signaling in the neocortex. Moreover,

279 phosphorylation of Akt at Serine^{473} has been implicated in inhibiting cilia assembly and promoting

280 cilia disassembly (Mao et al., 2019). We therefore investigated the amount of phospho-Akt^{S473} in

281 western blots on protein extracts from the E12.5 and E14.5 dorsal telencephalon. This analysis

282 revealed increased phosphorylation of Akt at Serine^{473} at E12.5 but no significant change at E14.5

283 (SupFig. 11). Since Akt acts upstream of mTOR (Yu & Cui, 2016), we also analysed the activity of

284 the mTOR pathway and investigated the phosphorylation of the S6 ribosomal protein, at Serine$^{235/236}$

285 and Serine$^{S240/244}$ (Ferrari, Bandi, Hofsteenge, Bussian, & Thomas, 1991). Interestingly, *Inpp5e*

286 mutants showed increased S6 phosphorylation at Serine$^{235/236}$ in E12.5 and E14.5 embryos whereas

287 an increase in phospho-S6$^{S240/244}$ remained restricted to E12.5 (SupFig. 11). Taken together, these

288 findings indicate that *Inpp5e* inactivation leads to increased activation of Akt and mTOR signaling in

289 the E12.5 dorsal telencephalon.

9

290   Next, we investigated a potential role of elevated mTOR signaling in controlling the balance

291   between direct and indirect neurogenesis and treated E11.5 pregnant mice with the mTORC1

292   inhibitor rapamycin (1mg/kg bodyweight). We harvested embryos 24h later and determined the

293   proportions of basal progenitors and neurons. This analysis revealed that administering rapamycin

294   did not rescue basal progenitor and neuron formation although the cortex of rapamycin treated

295   *Inpp5e*$^{\Delta/\Delta}$ embryos appeared elongated (SupFig. 11). Based on this experiment, augmented mTOR

296   signaling does not underlie the altered ratio of direct vs indirect neurogenesis in *Inpp5e*$^{\Delta/\Delta}$ embryos.

297

298   **Restoring Gli3 repressor ratio rescues cortical malformations in *Inpp5e*$^{\Delta/\Delta}$ embryos**

299   Primary cilia also play a crucial role in Shh signaling by controlling the proteolytic cleavage

300   of full length Gli3 (Gli3FL) into the Gli3 repressor form (Gli3R) in the absence of Shh and by

301   converting Gli3FL into the transcriptional activator Gli3A in the presence of Shh. Moreover, the dorsal

302   telencephalon predominately forms Gli3R (Fotaki, Yu, Zaki, Mason, & Price, 2006) and mice that

303   can only produce Gli3R have no obvious defect in cortical development (Besse et al., 2011; Böse,

304   Grotewold, & Rüther, 2002). In addition, we recently showed that Gli3 has a prominent role in radial

305   glial cells controlling the switch from symmetric proliferative to asymmetric neurogenic cell division

306   (Hasenpusch-Theil et al., 2018). Therefore, we hypothesized that alterations in Gli3 processing

307   caused by abnormal cilia function underlies the increased direct neurogenesis and the cortical

308   malformations in *Inpp5e*$^{\Delta/\Delta}$ embryos. In situ hybridization showed that *Gli3* mRNA expression might

309   be slightly reduced but the overall expression pattern in the telencephalon remains unaffected

310   (SupFig. 12). We next investigated the formation of Gli3FL and Gli3R in the E12.5 dorsal

311   telencephalon of *Inpp5e*$^{\Delta/\Delta}$ embryos using Western blots. This analysis revealed no change in the

312   levels of Gli3FL but a significant decrease inGli3R which resulted in a reduced Gli3R to Gli3FL ratio

313   in the mutant (Fig. 7A-D) suggesting that the *Inpp5e* mutation affects Gli3 processing.

314   The next set of experiments aimed to clarify a role for the reduced Gli3 processing. To this

315   end, we restored Gli3R levels by crossing *Inpp5e* mutants with *Gli3*$^{\Delta699/+}$ mice that can only produce

316   Gli3R in a cilia-independent manner (Besse et al., 2011; Böse et al., 2002). Overall inspection of

317   *Inpp5e*$^{\Delta/\Delta}$;*Gli3*$^{\Delta699/+}$ embryos revealed normal eye formation whereas *Inpp5e*$^{\Delta/\Delta}$ embryos either

318   completely lacked eyes or showed microphthalmia (Jacoby et al., 2009) (SupFig. 13). Moreover, the

319   overall morphology of the telencephalon is much improved in *Inpp5e*$^{\Delta/\Delta}$;*Gli3*$^{\Delta699/+}$ embryos as

320   compared to *Inpp5e*$^{\Delta/\Delta}$ embryos. In E18.5 *Inpp5e*$^{\Delta/\Delta}$ *Gli3*$^{\Delta699/+}$ mutants, the corpus callosum has a

321   thickness indistinguishable from that of control embryos (SupFig. 14). In E12.5 and E14.5

322   *Inpp5e*$^{\Delta/\Delta}$;*Gli3*$^{\Delta699/+}$ embryos, the neocortex lacks the undulations of the VZ present in *Inpp5e*$^{\Delta/\Delta}$

323   embryos (data not shown) and the morphology of the hippocampal anlage is more akin to that in

324   wild-type embryos but it is still smaller and less bulged (Fig. 7E, H, K, N).

325   We also determined the proportions of basal progenitors and Tbr1+ neurons at E12.5 which

326   were decreased and increased, respectively, in the lateral neocortex of *Inpp5e*$^{\Delta/\Delta}$ embryos.

10

327   Remarkably, there was no statistically significant difference between control and $Inpp5e^{\Delta/\Delta}$;$Gli3^{\Delta699/+}$

328   embryos (Fig. 7E-J) indicating that the neurogenesis phenotype of E12.5 $Inpp5e^{\Delta/\Delta}$ mutants is

329   rescued by a single copy of the $Gli3^{\Delta699}$ allele. The proportion of Tbr1+Ctip2+ neurons was not

330   affected in the medial neocortex of E14.5 $Inpp5e^{\Delta/\Delta}$;$Gli3^{\Delta699/+}$ embryos (Fig. 7K, M, N) either, however,

331   the proportion of Tbr1-Ctip2+ neurons was reduced (Fig. 7K, N, P). Similarly, the proportions of basal

332   progenitors in the E14.5 medial neocortex was reduced in $Inpp5e^{\Delta/\Delta}$ $Gli3^{\Delta699/+}$ embryos as in $Inpp5e^{\Delta/\Delta}$

333   embryos (Fig. 7L, O, S). As re-introducing a single $Gli3^{\Delta699}$ allele does not completely rescue the

334    $Inpp5e^{\Delta/\Delta}$ neurogenesis phenotype, we generated $Inpp5e^{\Delta/\Delta}$ embryos homozygous for $Gli3^{\Delta699}$.

335   Interestingly, the morphology of the telencephalon including the hippocampal formation was

336   indistinguishable between control and $Inpp5e^{\Delta/\Delta}$;$Gli3^{\Delta699/\Delta699}$ embryos (Fig. 7K, Q) and the proportions

337   of Tbr1-Ctip2+ and basal progenitors were not affected any longer (Fig. 7K, L. P-S). Taken together,

338   these findings indicate that re-introducing a single copy of the $Gli3R$ allele into the $Inpp5e$ mutant

339   background leads to a partial rescue of cortical neurogenesis in $Inpp5e^{\Delta/\Delta}$ embryos whereas two

340   copies are required for a full rescue.

341

DISCUSSION

Generating a functional cerebral cortex requires a finely tuned balance between direct and indirect neurogenesis to form subtypes of cortical projection neurons in appropriate numbers. Here, we show that the ciliary mouse mutants *Inpp5e* and *Tctn2* present with a transient increase in neurons forming directly from radial glia progenitors in the lateral neocortex at the expense of basal progenitor formation. This increase in neurogenesis results in augmented formation of Ctip2+ layer V neurons in the *Inpp5e* mutant cortex. Our studies also revealed that the *Inpp5e* mutation interfered with the stability of the RGC primary cilium and its signaling functions, leading to a reduction in the Gli3R levels. Since re-introducing Gli3R in an *Inpp5e* mutant background restored the decreased formation of normal proportions of basal progenitors and neurons, our findings implicate a novel role for primary cilia in controlling the signaling events that direct the decision of RGCs to undergo either direct or indirect neurogenesis.

Primary cilia affect the decision between direct and indirect neurogenesis

Radial glial cells in the developing mouse neocortex have the potential to undergo symmetric proliferative or asymmetric cell divisions with the latter division mode producing neurons in a direct manner or indirectly via basal progenitors. Balancing out these division modes is important not only to determine final neuronal output and cortical size but also the types of cortical projection neurons and, hence, subtype composition of the adult neocortex. In the E12.5 *Inpp5e* and *Tctn2* mouse mutants, we identified an increased formation of neurons in the lateral neocortex. Based on our cell cycle exit experiment additional neurons are formed from RGCs at the expense of basal progenitors. Given the cell cycle length of basal progenitors of >24 hours (Arai et al., 2011), it is unlikely that new born basal progenitors would have undergone an additional round of cell division to produce two neurons within the time frame of this experiment. Such an extra division would also have diluted the BrdU label. We therefore conclude that the *Inpp5e* mutation caused RGCs to preferentially produce neurons directly.

Interestingly, this increase in direct neurogenesis led to an increased proportion of Ctip2+ deep layer V neurons in the E18.5 neocortex but did not coincide with a reduced proportion of upper layer neurons. This effect could be explained in several mutually non-exclusive ways. First, neurons born at E12.5 initially express both Ctip2 and Tbr1 (Fig. 7) and later down-regulate Ctip2. *Inpp5e* could therefore affect the signaling that controls this downregulation. Secondly, the proportions of basal progenitors and neurons was normalized in E14.5 mutants. Since basal progenitors are a main source of upper layer neurons (Arnold et al., 2008; Vasistha et al., 2015), this normalization would account for the sufficient numbers of Satb2+ upper layer neurons. Newly formed projection neurons signal back to RGCS via Jag1, Fgf9 and Neurotrophin 3 (Parthasarathy et al., 2014; Seuntjens et al., 2009; W. Wang et al., 2016) to control the sequential production of deep and upper layer neurons and of glia (Silva et al., 2019). *Inpp5e* might affect these signals by controlling cilia stability and/or levels of PI(3,4,5)P_3 (Bielas et al., 2009; Jacoby et al., 2009) that acts as a second messenger in

12

380 receptor tyrosine kinase signaling. This possibility is supported by our observation that the extent of

381 the pErk expression domain in the neocortex is diminished in E14.5 *Inpp5e*$^{\Delta/\Delta}$ embryos. Regardless

382 of the exact mechanism, our findings suggest a novel, spatially and temporally restricted role for

383 *Inpp5e* in controlling the decision between direct and indirect neurogenesis. This function differs from

384 those described for other cilia mutants. Conditional inactivation of *Ift88* and *Kif3a* leads to a larger

385 cortex (Foerster et al., 2017; Wilson et al., 2012) with a modest increase in BP production in the

386 absence of a delay in neurogenesis (Foerster et al., 2017) while *Rpgrip1l* mutants have reduced

387 numbers of both basal progenitors and neurons (Postel, Karam, Pezeron, Schneider-Maunoury, &

388 Clement, 2019). These findings highlight the multiple and varied roles cilia play in cortical

389 development.

390

391 **Inpp5e controls direct/indirect neurogenesis through Gli3 processing**

392   Our study also shed lights into the mechanisms by which *Inpp5e* controls the decision

393 between direct/indirect neurogenesis. Most notably, the Gli3R level and Gli3R/Gli3FL ratio are

394 decreased in *Inpp5e*$^{\Delta/\Delta}$ embryos. While the *Inpp5e* mutation does not lead to an up-regulation of Shh

395 signaling in the dorsal telencephalon (Magnani et al., 2015), re-introducing a single or two copies of

396 Gli3R in an *Inpp5e* mutant background partially and fully restores the neurogenesis defects,

397 respectively. This rescue indicates that reduced levels of Gli3R rather than the reduction in the

398 Gli3R/Gli3FL ratio are responsible for the prevalence of direct neurogenesis in *Inpp5e*$^{\Delta/\Delta}$ embryos.

399 This idea is consistent with the findings that (i) *Gli3*$^{\Delta699/\Delta699}$ embryos that cannot produce Gli3FL and

400 Gli3A show no obvious phenotype in cortical development (Besse et al., 2011; Böse et al., 2002),

401 (ii) dorsal telencephalic patterning defects in *Gli3*$^{Xt/Xt}$ mutants are not rescued in *Shh*$^{-/-}$/*Gli3*^{XtXt} double

402 mutants (Rallu et al., 2002; Rash & Grove, 2007), (iii) Shh promotes the generation of olfactory bulb

403 interneurons and cortical oligodendrocytes and neurogenesis in the subventricular zone by reducing

404 Gli3R rather than by promoting Gli activator function (Petrova, Garcia, & Joyner, 2013; H. Wang,

405 Kane, Lee, & Ahn, 2014; Zhang et al., 2020). In addition, there is also a dramatic rescue of eye

406 development and the rescue also extends to other malformations of the *Inpp5e*$^{\Delta/\Delta}$ forebrain, including

407 the corpus callosum, the hippocampus and the expansion of the piriform cortex, structures that are

408 also affected in *Gli3* null and hypomorphic mutants (Amaniti et al., 2015; Johnson, 1967; Magnani

409 et al., 2014; Theil, Alvarez-Bolado, Walter, & Rüther, 1999; Wiegering, Petzsch, Kohrer, Ruther, &

410 Gerhardt, 2019). Taken together, these findings support the idea that *Inpp5e* and the primary cilium

411 control key processes in cortical development by regulating the formation of Gli3R.

412   Our analyses support several mutually non-exclusive mechanisms how the *Inpp5e* mutation

413 impacts on Gli3 processing. First, our electron microscopy study revealed severe structural

414 abnormalities in large proportions of cilia. The Inpp5e phosphatase hydrolyses PI(3,4,5)P$_3$, which is

415 essential for the effective activation of the serine threonine kinase Akt (Kisseleva et al., 2002;

416 Plotnikova et al., 2015). Following PIP3 binding, Akt translocates to the membrane and becomes

417 phosphorylated at T308 by phosphoinositide dependent kinase-1 (Pdk1) and at S473 by mammalian

13

418   target of rapamycin complex (mTORC2) (Yu & Cui, 2016). Consistent with the loss of *Inpp5e* function

419   and a resulting increase in PI(3,4,5)P$_3$, our western blot analysis revealed elevated pAkt^{S473} levels.

420   Increased phosphorylation at this site has been implicated in inhibiting cilia assembly and promoting

421   cilia disassembly (Mao et al., 2019) and could hence explain the structural defects of RGC *Inpp5e*$^{\Delta/\Delta}$

422   cilia. Secondly, *Inpp5e* could control Gli3 processing through its effect on the transition zone (TZ). It

423   is required for TZ molecular organisation (Dyson et al., 2017) and its substrate PI(4,5)P2 plays a

424   role in TZ maturation in Drosophila (Gupta, Fabian, & Brill, 2018). This model is further supported by

425   our finding that a mouse mutant for the TZ protein Tctn2 phenocopies the *Inpp5e*$^{\Delta/\Delta}$ neurogenesis

426   defect. In turn, several mouse mutants defective for TZ proteins show microphthalmia (Garcia-

427   Gonzalo et al., 2011; Sang et al., 2011; Yee et al., 2015). Tctn proteins are also required for Gli3

428   processing (Sang et al., 2011; Thomas et al., 2012; C. Wang, Li, Meng, & Wang, 2017) and the TZ

429   protein Rpgrip1l controls the activity of the proteasome at the basal body responsible for proteolytic

430   cleavage of Gli3 (Gerhardt et al., 2015). Taken together, these findings indicate that *Inpp5e* mutation

431   might affect the ability of RGCs to switch to indirect neurogenesis through defects in cilia stability

432   and/or the integrity of the ciliary transition zone.

433

434   **Implications for Joubert Syndrome**

435   In humans, hypomorphic *INPP5E* mutations contribute to Joubert Syndrome (JS), a

436   ciliopathy characterized by cerebellar malformations and concomitant ataxia and breathing

437   abnormalities. In addition, a subset of JS patients exhibit cortical abnormalities including

438   polymicrogyria, neuronal heterotopias and agenesis of the corpus callosum (Poretti, Huisman,

439   Scheer, & Boltshauser, 2011). Strikingly, the *Inpp5e* mouse mutant also shows several of these

440   abnormalities. In the caudal telencephalon, the otherwise lissencephalic cortex formed folds

441   reminiscent of the polymicrogyria in JS patients. In addition, the mutant formed leptomeningeal

442   heterotopias with 100% penetrance, but their number and location varied. Mutations in ciliary genes

443   were previously associated with heterotopia formation in humans and mice (Magnani et al., 2015;

444   Uzquiano et al., 2019). Mice carrying mutations in the *Eml1* gene encoding a microtubule-associated

445   protein show subcortical heterotopias due to a mispositioning of radial glial cells and impaired

446   primary cilia formation (Uzquiano et al., 2019). Finally, the corpus callosum is thinner but callosal

447   axons normally project to the contralateral cerebral hemisphere in *Inpp5e* mutants. This phenotype

448   is milder compared to that of other mouse mutants with altered cilia that show complete agenesis of

449   the corpus callosum with callosal axons forming Probst bundles (Benadiba et al., 2012; Laclef et al.,

450   2015; Putoux et al., 2019). Unlike these other ciliary mutants, the corticoseptal boundary which plays

451   a crucial role in positioning guidepost cells that control midline crossing of callosal axons (Magnani

452   et al., 2014) is not obviously affected in *Inpp5e*$^{\Delta/\Delta}$ embryos. Instead, the thinner corpus callosum is

453   likely to be the result of an expanded piriform cortex. Despite these mechanistic differences,

454   however, re-introducing Gli3R into the cilia mutant background restores callosal development in both

455   groups of mutants suggesting that cilia control two independent steps in corpus callosum formation

456   by regulating Gli3 processing. Thus, the *Inpp5e*$^{\Delta/\Delta}$ mutant recapitulates cortical abnormalities in JS

457   patients and starts to help unravelling the pathomechanisms underlying these defects.

458

15

MATERIAL & METHODS

Mice

All experimental work was carried out in accordance with the UK Animals (Scientific Procedures) Act 1986 and UK Home Office guidelines. All protocols were reviewed and approved by the named veterinary surgeons of the College of Medicine and Veterinary Medicine, the University of Edinburgh, prior to the commencement of experimental work. $Inpp5e^{\Delta/+}$ and $Gli3^{\Delta699/+}$ mouse lines have been described previously (Böse et al., 2002; Jacoby et al., 2009). $Inpp5e^{\Delta/+}$ mice were interbred to generate $Inpp5e^{\Delta/\Delta}$ embryos; exencephalic $Inpp5e^{\Delta/\Delta}$ embryos were excluded from the analyses. Wild-type and $Inpp5e^{\Delta/+}$ litter mate embryos served as controls. $Inpp5e^{\Delta/\Delta};Gli3^{\Delta699/+}$ and $Inpp5e^{\Delta/\Delta};Gli3^{\Delta699/\Delta699}$ embryos were obtained from inter-crosses of $Inpp5e^{\Delta/+};Gli3^{\Delta699/+}$ mice using wild-type, $Inpp5e^{\Delta/+}$ and $Gli3^{\Delta699/+}$ embryos as controls. Embryonic (E) day 0.5 was assumed to start at midday of the day of vaginal plug discovery. Transgenic animals and embryos were genotyped as described (Böse et al., 2002; Jacoby et al., 2009). For each marker and each stage, 3-8 embryos were analysed.

For measuring cell cycle lengths, pregnant females were intraperitoneally injected with a single dose of IdU (10mg/ml) at E12.5, followed by an injection of BrdU (10mg/ml) 90 min later. Embryos were harvested 30 min after the second injection. For cell cycle exit analyses, BrdU was injected peritoneally into E11.5 pregnant females and embryos were harvested 24 hrs later. Rapamycin was dissolved in 100% EtOH and diluted in vehicle containing 5% PEG400, 5% Tween80 immediately before use. E11.5 pregnant females received a single intraperitoneal injection of Rapamycin at 1 mg/kg body weight or of vehicle and were killed 24 hrs later.

Immunohistochemistry and in situ hybridisation

For immunohistochemistry, embryos were fixed overnight in 4% paraformaldehyde, incubated in 30% sucrose at +4°C for 24h, embedded in 30% sucrose/OCT mixture (1:1) and frozen on dry ice. Immunofluorescence staining was performed on 12 to 14 μm cryostat sections as described previously (Theil, 2005) with antibodies against Arl13b (Neuromab 75-287; 1:1500), rabbit anti-BrdU (1:50, Abcam #ab6326), mouse anti-BrdU/IdU (B44) (1:50, BD Biosciences #347580), rat anti-Ctip2 (1:1000, Abcam #18465), rabbit anti-pErk$^{T202/Y204}$ (1:1000, Cell Signaling Technology #9101), rabbit anti-GFAP (1:1000, Dako #Z 0334), rat anti-L1, clone 324 (1:1000, Millipore #MAB5272), rabbit anti-Pax6 (1:400, Biolegend #901301), mouse anti-PCNA (1:500, Abcam #29), rabbit anti-Prox1 (1:1000, RELIA*Tech* #102-PA32). rabbit anti-pHH3 (1:100, Millipore #06-570), mouse anti-Satb2 (1:200, Abcam #51502), rabbit anti-Tbr1 (1:400, Abcam #31940), rabbit anti-Tbr2 (1:1000, Abcam #23345) and γTUB (Sigma T6557; 1:2000). Primary antibodies for immunohistochemistry were detected with Alexa- or Cy2/3-conjugated fluorescent secondary antibodies. The Tbr1 signals were amplified using biotinylated secondary IgG antibody (swine anti-rabbit IgG) (1:400, BD Biosciences) followed by

16

496 Alexa Fluor 488 or 568 Streptavidin (1:100, Invitrogen). For counter staining DAPI (1:2000, Life

497 Technologies) was used. Prox1 and pErk$^{T202/Y204}$ proteins were detected non-fluorescently using

498 biotinylated goat anti-rabbit IgG (1: 400, BD Biosciences) followed by avidin-HRP and DAB detection

499 (Vector labs) as described previously (Magnani et al., 2010).

500 In situ hybridisation on 12μm serial paraffin sections were performed as described previously (Theil,

501 2005) using antisense RNA probes for *Axin2* (Lustig et al., 2002), *Bmp4* (Jones, Lyons, & Hogan,

502 1991), *Dbx1* (Yun, Potter, & Rubenstein, 2001), *Dlx2* (Bulfone et al., 1993), *Emx1* (Simeone et al.,

503 1992), *Gli3* (Hui, Slusarski, Platt, Holmgren, & Joyner, 1994), *Lhx2* (Liem, Tremml, & Jessell, 1997),

504 *Msx1 (Hill et al., 1989)*, *Ngn2* (Gradwohl, Fode, & Guillemot, 1996), *Nrp2* (Galceran et al., 2000),

505 *Pax6* (Walther & Gruss, 1991), *Scip1* (Frantz et al., 1994), *Wnt2b* (Grove, Tole, Limon, Yip, &

506 Ragsdale, 1998).

507

508 **Western blot**

509 Protein was extracted from the dorsal telencephalon of E12.5 (3 tissues pooled per sample) and

510 E14.5 (single tissue per sample) wild-type and *Inpp5e*$^{\Delta/\Delta}$ embryos (n=4 samples per genotype) as

511 described previously (Magnani et al., 2010). For the detection of Gli3 10µg protein lysates were

512 subjected to gel electrophoresis on a 3-8% NuPAGE® Tris-Acetate gel (Life Technologies), and

513 protein was transferred to a Immobilon-FL membrane (Millipore), which was incubated with goat

514 anti-h/m Gli3 (1:500, R&D Systems #AF3690) and mouse anti-β-Actin antibody (1:15000, Abcam

515 #ab6276). After incubating with donkey anti-goat IgG IRDye680RD (1:15000, LI-COR Biosciences)

516 and donkey anti-mouse IgG IRDye800CW secondary antibodies (1:15000, Life Technologies),

517 signal was detected using LI-COR's Odyssey Infrared Imaging System with Odyssey Software.

518 Values for protein signal intensity were obtained using Image Studio Lite Version3.1. Gli3 repressor

519 and activator protein levels were compared between wild-type and mutant tissue using a paired t-

520 test.

521 For all other Western blot analyses 20µg protein lysates were loaded on 4–12% NuPAGE® Bis-Tris

522 gels (Life Technologies) and later transferred to an Immobilon–FL membrane. Membranes were

523 incubated with the following primary antibodies: rabbit anti-phospho-Akt^{S473} (1:1000, Cell Signaling

524 Technologies CST #9271), rabbit anti-Akt (1:1000, CST #9272), rabbit anti-phospho-Erk$^{T202/Y204}$

525 (1:1000, CST #9101), rabbit anti-Erk (L34F12) (CST # 4696), rabbit anti-ribosomal protein phospho-

526 S6$^{S235/S236}$ (1:1000, CST #2211), rabbit anti-ribosomal protein phospho-S6$^{S240/S244}$ (1:1000, CST

527 #2215) and mouse anti-ribosomal protein S6 (C-8) (1:1000, Santa Cruz Technologies #sc-74459).

528 For the detection of phosphorylated proteins goat anti-rabbit IRDye 680RD (1:15,000, LI-COR

529 Biosciences) and for total proteins goat anti-mouse or goat anti-rabbit IRDye 800CW (1:15,000, LI-

530 COR Biosciences) were used as secondary antibodies. The signals were detected via the Odyssey

531 Imaging System and further analysed using Image Studio Lite Version4.0. The ratios between

532 phosphorylated and total protein were compated between wild-type and mutant tissue using a paired

533 t-test.

17

534

Scanning and transmission electron microscopy

536 TEM and SEM image acquisition were performed in the Cochin Imaging Facility and on the IBPS

537 EM Facility, respectively. For scanning electron microscopy, embryos were dissected in 1.22x PBS

538 (pH 7.4) and fixed overnight with 2% glutaraldehyde in 0.61x PBS (pH 7.4) at 4°C. Heads were then

539 sectioned to separate the dorsal and ventral parts of the telencephalon, exposing their ventricular

540 surfaces. Head samples were washed several times in 1.22x PBS and postfixed for 15 minutes in

541 1.22x PBS containing 1% OsO4. Fixed samples were washed several times in ultrapure water,

542 dehydrated with a graded series of ethanol and prepared for scanning electron microscopy using the

543 critical point procedure (CPD7501, Polaron). Their surfaces were coated with a 20 nm gold layer

544 using a gold spattering device (Scancoat Six, Edwards). Samples were observed under a Cambridge

545 S260 scanning electron microscope at 10 keV.

546 For transmission electron microscopy tissues were fixed for 1 hour with 3% glutaraldehyde, post-

547 fixed in 1.22x PBS containing 1% OsO4, then dehydrated with a graded ethanol series. After 10

548 minutes in a 1:2 mixture of propane:epoxy resin, tissues were embedded in gelatin capsules with

549 freshly prepared epoxy resin and polymerized at 60°C for 24 hours. Sections (80 nm) obtained using

550 an ultramicrotome (Reichert Ultracut S) were stained with uranyl acetate and Reynold's lead citrate

551 and observed with a Philips CM10 transmission electron microscope.

552

Statistical Analyses

554 Data were analysed using GraphPadPrism 6 software with n=3-8 embryos for all analyses. Power

555 analysis of pilot experiments informed minimum samples size. Mann Whitney tests were performed

556 for immunohistochemical analyses in general. Cortical thickness was analysed using a two way

557 ANOVA followed by Sidak's multiple comparisons test. Paired t-tests were performed for Western

558 blots and a fisher's exact test was used to analyse the quantification of normal and abnormal cilia.

559 The mTORC1 and Gli3 rescue experiments were evaluated with one way ANOVAS followed by

560 Tukey's multiple comparisons test. A single asterisk indicates significance of $p<0.05$, two asterisks

561 indicate significance of $p<0.01$ and three asterisks of $p<0.005$. Due to morphological changes

562 blinding was not possible and scores were validated by a second independent observer.

563

564

ACKNOWLEDGEMENTS

566

575

576   **COMPETING INTERESTS**

577

578   The authors declare no competing interests.

579

580

581

REFERENCES

Amaniti, E. M., Fu, C., Lewis, S., Saisana, M., Magnani, D., Mason, J. O., & Theil, T. (2015). Expansion of the piriform cortex contributes to corticothalamic pathfinding defects in Gli3 conditional mutants. *Cereb Cortex, 25*(2), 460-471. doi:10.1093/cercor/bht244

Arai, Y., Pulvers, J. N., Haffner, C., Schilling, B., Nusslein, I., Calegari, F., & Huttner, W. B. (2011). Neural stem and progenitor cells shorten S-phase on commitment to neuron production. *Nature communications, 2*, 154. doi:10.1038/ncomms1155

Ariens-Kapers, C. U., Huber, G. C., & Crosby, E. C. (1936). The comparative anatomy of the nervous system of the vertebrates including man. *New York Macmillan*.

Arnold, S. J., Huang, G. J., Cheung, A. F., Era, T., Nishikawa, S., Bikoff, E. K., . . . Groszer, M. (2008). The T-box transcription factor Eomes/Tbr2 regulates neurogenesis in the cortical subventricular zone. *Genes Dev, 22*(18), 2479-2484. doi:10.1101/gad.475408

Ashique, A. M., Choe, Y., Karlen, M., May, S. R., Phamluong, K., Solloway, M. J., . . . Peterson, A. S. (2009). The Rfx4 transcription factor modulates Shh signaling by regional control of ciliogenesis. *Sci Signal, 2*(95), ra70. doi:10.1126/scisignal.2000602

Benadiba, C., Magnani, D., Niquille, M., Morle, L., Valloton, D., Nawabi, H., . . . Durand, B. (2012). The ciliogenic transcription factor RFX3 regulates early midline distribution of guidepost neurons required for corpus callosum development. *PLoS genetics, 8*(3), e1002606. doi:10.1371/journal.pgen.1002606

Besse, L., Neti, M., Anselme, I., Gerhardt, C., Ruther, U., Laclef, C., & Schneider-Maunoury, S. (2011). Primary cilia control telencephalic patterning and morphogenesis via Gli3 proteolytic processing. *Development, 138*(10), 2079-2088. doi:10.1242/dev.059808

Bielas, S. L., Silhavy, J. L., Brancati, F., Kisseleva, M. V., Al-Gazali, L., Sztriha, L., . . . Gleeson, J. G. (2009). Mutations in INPP5E, encoding inositol polyphosphate-5-phosphatase E, link phosphatidyl inositol signaling to the ciliopathies. *Nat Genet, 41*(9), 1032-1036. doi:10.1038/ng.423

Böse, J., Grotewold, L., & Rüther, U. (2002). Pallister-Hall syndrome phenotype in mice mutant for Gli3. *Hum Mol Genet, 11*(9), 1129-1135.

Bulfone, A., Puelles, L., Porteus, M. H., Frohman, M. A., Martin, G. R., & Rubenstein, J. L. (1993). Spatially restricted expression of Dlx-1, Dlx-2 (Tes-1), Gbx-2, and Wnt-3 in the embryonic day 12.5 mouse forebrain defines potential transverse and longitudinal segmental boundaries. *J Neurosci, 13*(7), 3155-3172.

Cardenas, A., Villalba, A., de Juan Romero, C., Pico, E., Kyrousi, C., Tzika, A. C., . . . Borrell, V. (2018). Evolution of Cortical Neurogenesis in Amniotes Controlled by Robo Signaling Levels. *Cell, 174*(3), 590-606 e521. doi:10.1016/j.cell.2018.06.007

Caspary, T., Larkins, C. E., & Anderson, K. V. (2007). The graded response to Sonic Hedgehog depends on cilia architecture. *Developmental cell, 12*(5), 767-778. doi:10.1016/j.devcel.2007.03.004

Chavez, M., Ena, S., Van Sande, J., de Kerchove d'Exaerde, A., Schurmans, S., & Schiffmann, S. N. (2015). Modulation of Ciliary Phosphoinositide Content Regulates Trafficking and Sonic Hedgehog Signaling Output. *Developmental cell, 34*(3), 338-350. doi:10.1016/j.devcel.2015.06.016

Dyson, J. M., Conduit, S. E., Feeney, S. J., Hakim, S., DiTommaso, T., Fulcher, A. J., . . . Mitchell, C. A. (2017). INPP5E regulates phosphoinositide-dependent cilia transition zone function. *J Cell Biol, 216*(1), 247-263. doi:10.1083/jcb.201511055

Englund, C., Fink, A., Lau, C., Pham, D., Daza, R. A., Bulfone, A., . . . Hevner, R. F. (2005). Pax6, Tbr2, and Tbr1 are expressed sequentially by radial glia, intermediate progenitor cells, and postmitotic neurons in developing neocortex. *J Neurosci, 25*(1), 247-251.

Ferrari, S., Bandi, H. R., Hofsteenge, J., Bussian, B. M., & Thomas, G. (1991). Mitogen-activated 70K S6 kinase. Identification of in vitro 40 S ribosomal S6 phosphorylation sites. *J Biol Chem, 266*(33), 22770-22775.

Florio, M., & Huttner, W. B. (2014). Neural progenitors, neurogenesis and the evolution of the neocortex. *Development, 141*(11), 2182-2194. doi:10.1242/dev.090571

636 Foerster, P., Daclin, M., Asm, S., Faucourt, M., Boletta, A., Genovesio, A., & Spassky, N. (2017).
637   mTORC1 signaling and primary cilia are required for brain ventricle morphogenesis.
638   *Development, 144*(2), 201-210. doi:10.1242/dev.138271
639 Fotaki, V., Yu, T., Zaki, P. A., Mason, J. O., & Price, D. J. (2006). Abnormal positioning of
640   diencephalic cell types in neocortical tissue in the dorsal telencephalon of mice lacking
641   functional Gli3. *J Neurosci, 26*(36), 9282-9292.
642 Frantz, G. D., Bohner, A. P., Akers, R. M., & McConnell, S. K. (1994). Regulation of the POU
643   domain gene SCIP during cerebral cortical development. *J Neurosci, 14*(2), 472-485.
644 Galceran, J., Miyashita-Lin, E. M., Devaney, E., Rubenstein, J. L., & Grosschedl, R. (2000).
645   Hippocampus development and generation of dentate gyrus granule cells is regulated by
646   LEF1. *Development, 127*(3), 469-482.
647 Garcia-Gonzalo, F. R., Corbit, K. C., Sirerol-Piquer, M. S., Ramaswami, G., Otto, E. A., Noriega, T.
648   R., . . . Reiter, J. F. (2011). A transition zone complex regulates mammalian ciliogenesis
649   and ciliary membrane composition. *Nat Genet, 43*(8), 776-784. doi:10.1038/ng.891
650 Garcia-Gonzalo, F. R., Phua, S. C., Roberson, E. C., Garcia, G., 3rd, Abedin, M., Schurmans, S., .
651   . . Reiter, J. F. (2015). Phosphoinositides Regulate Ciliary Protein Trafficking to Modulate
652   Hedgehog Signaling. *Developmental cell, 34*(4), 400-409. doi:10.1016/j.devcel.2015.08.001
653 Gerhardt, C., Lier, J. M., Burmuhl, S., Struchtrup, A., Deutschmann, K., Vetter, M., . . . Ruther, U.
654   (2015). The transition zone protein Rpgrip1l regulates proteasomal activity at the primary
655   cilium. *J Cell Biol, 210*(1), 115-133. doi:10.1083/jcb.201408060
656 Gladwyn-Ng, I., Cordon-Barris, L., Alfano, C., Creppe, C., Couderc, T., Morelli, G., . . . Nguyen, L.
657   (2018). Stress-induced unfolded protein response contributes to Zika virus-associated
658   microcephaly. *Nature neuroscience, 21*(1), 63-71. doi:10.1038/s41593-017-0038-4
659 Götz, M., Stoykova, A., & Gruss, P. (1998). Pax6 controls radial glia differentiation in the cerebral
660   cortex. *Neuron, 21*(5), 1031-1044.
661 Gradwohl, G., Fode, C., & Guillemot, F. (1996). Restricted expression of a novel murine atonal-
662   related bHLH protein in undifferentiated neural precursors. *Dev Biol, 180*(1), 227-241.
663 Grove, E. A., Tole, S., Limon, J., Yip, L., & Ragsdale, C. W. (1998). The hem of the embryonic
664   cerebral cortex is defined by the expression of multiple Wnt genes and is compromised in
665   Gli3-deficient mice. *Development, 125*(12), 2315-2325.
666 Gupta, A., Fabian, L., & Brill, J. A. (2018). Phosphatidylinositol 4,5-bisphosphate regulates cilium
667   transition zone maturation in Drosophila melanogaster. *J Cell Sci, 131*(16).
668   doi:10.1242/jcs.218297
669 Hall, P. A., Levison, D. A., Woods, A. L., Yu, C. C., Kellock, D. B., Watkins, J. A., . . . et al. (1990).
670   Proliferating cell nuclear antigen (PCNA) immunolocalization in paraffin sections: an index
671   of cell proliferation with evidence of deregulated expression in some neoplasms. *J Pathol,*
672   *162*(4), 285-294. doi:10.1002/path.1711620403
673 Hasenpusch-Theil, K., West, S., Kelman, A., Kozic, Z., Horrocks, S., McMahon, A. P., . . . Theil, T.
674   (2018). Gli3 controls the onset of cortical neurogenesis by regulating the radial glial cell
675   cycle through Cdk6 expression. *Development, 145*(17). doi:10.1242/dev.163147
676 Haubensak, W., Attardo, A., Denk, W., & Huttner, W. B. (2004). Neurons arise in the basal
677   neuroepithelium of the early mammalian telencephalon: a major site of neurogenesis. *Proc*
678   *Natl Acad Sci U S A, 101*(9), 3196-3201.
679 Hill, R. E., Jones, P. F., Rees, A. R., Sime, C. M., Justice, M. J., Copeland, N. G., . . . Davidson, D.
680   R. (1989). A new family of mouse homeo box-containing genes: molecular structure,
681   chromosomal location, and developmental expression of Hox-7.1. *Genes Dev, 3*(1), 26-37.
682 Hui, C. C., Slusarski, D., Platt, K. A., Holmgren, R., & Joyner, A. L. (1994). Expression of three
683   mouse homologs of the Drosophila segment polarity gene cubitus interruptus, Gli, Gli-2,
684   and Gli-3, in ectoderm- and mesoderm-derived tissues suggests multiple roles during
685   postimplantation development. *Dev Biol, 162*(2), 402-413.
686 Jacoby, M., Cox, J. J., Gayral, S., Hampshire, D. J., Ayub, M., Blockmans, M., . . . Schurmans, S.
687   (2009). INPP5E mutations cause primary cilium signaling defects, ciliary instability and
688   ciliopathies in human and mouse. *Nat Genet, 41*(9), 1027-1031.
689 Johnson, D. R. (1967). Extra-toes: a new mutant gene causing multiple abnormalities in the
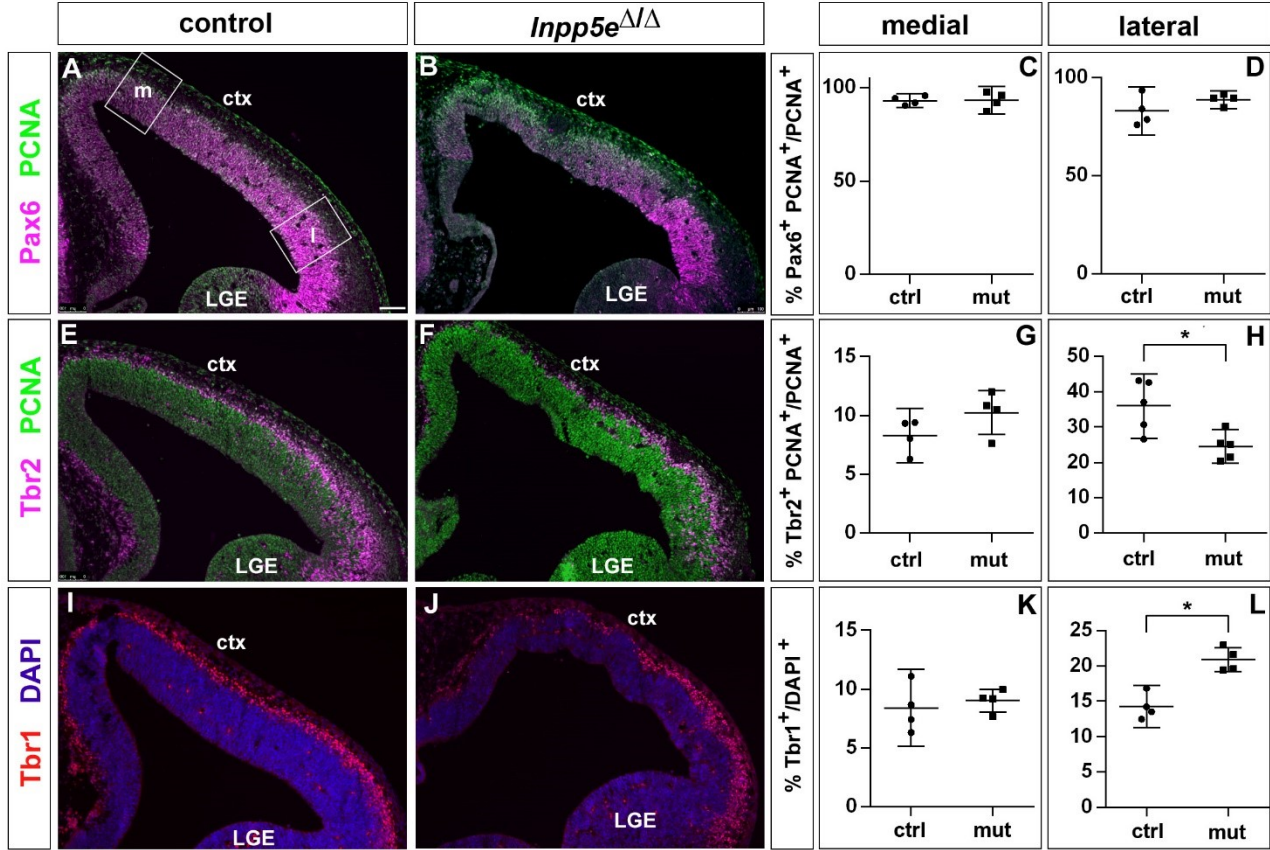690   mouse. *J Embryol Exp Morphol, 17*(3), 543-581.

691 Jones, C. M., Lyons, K. M., & Hogan, B. L. (1991). Involvement of Bone Morphogenetic Protein-4
692   (BMP-4) and Vgr-1 in morphogenesis and neurogenesis in the mouse. *Development,*
693   *111*(2), 531-542.
694 Kisseleva, M. V., Cao, L., & Majerus, P. W. (2002). Phosphoinositide-specific inositol
695   polyphosphate 5-phosphatase IV inhibits Akt/protein kinase B phosphorylation and leads to
696   apoptotic cell death. *J Biol Chem, 277*(8), 6266-6272. doi:10.1074/jbc.M105969200
697 Laclef, C., Anselme, I., Besse, L., Catala, M., Palmyre, A., Baas, D., . . . Schneider-Maunoury, S.
698   (2015). The role of primary cilia in corpus callosum formation is mediated by production of
699   the Gli3 repressor. *Hum Mol Genet, 24*(17), 4997-5014. doi:10.1093/hmg/ddv221
700 Laguesse, S., Creppe, C., Nedialkova, D. D., Prevot, P. P., Borgs, L., Huysseune, S., . . . Nguyen,
701   L. (2015). A Dynamic Unfolded Protein Response Contributes to the Control of Cortical
702   Neurogenesis. *Developmental cell, 35*(5), 553-567. doi:10.1016/j.devcel.2015.11.005
703 Lee, S. M., Tole, S., Grove, E., & McMahon, A. P. (2000). A local Wnt-3a signal is required for
704   development of the mammalian hippocampus. *Development, 127*(3), 457-467.
705 Liem, K. F., Jr., Tremml, G., & Jessell, T. M. (1997). A role for the roof plate and its resident
706   TGFbeta-related proteins in neuronal patterning in the dorsal spinal cord. *Cell, 91*(1), 127-
707   138.
708 Lustig, B., Jerchow, B., Sachs, M., Weiler, S., Pietsch, T., Karsten, U., . . . Behrens, J. (2002).
709   Negative Feedback Loop of Wnt Signaling through Upregulation of Conductin/Axin2 in
710   Colorectal and Liver Tumors. *Mol. Cell. Biol., 22*(4), 1184-1193.
711 Magnani, D., Hasenpusch-Theil, K., Benadiba, C., Yu, T., Basson, M. A., Price, D. J., . . . Theil, T.
712   (2014). Gli3 controls corpus callosum formation by positioning midline guideposts during
713   telencephalic patterning. *Cerebral cortex, 24*(1), 186-198. doi:10.1093/cercor/bhs303
714 Magnani, D., Hasenpusch-Theil, K., Jacobs, E. C., Campagnoni, A. T., Price, D. J., & Theil, T.
715   (2010). The Gli3 hypomorphic mutation Pdn causes selective impairment in the growth,
716   patterning, and axon guidance capability of the lateral ganglionic eminence. *J Neurosci,*
717   *30*(41), 13883-13894. doi:30/41/13883 [pii]
718 10.1523/JNEUROSCI.3650-10.2010
719 Magnani, D., Morle, L., Hasenpusch-Theil, K., Paschaki, M., Jacoby, M., Schurmans, S., . . . Theil,
720   T. (2015). The ciliogenic transcription factor Rfx3 is required for the formation of the
721   thalamocortical tract by regulating the patterning of prethalamus and ventral telencephalon.
722   *Hum Mol Genet, 24*(9), 2578-2593. doi:10.1093/hmg/ddv021
723 Mao, H., Tang, Z., Li, H., Sun, B., Tan, M., Fan, S., . . . Sun, Y. (2019). Neddylation inhibitor
724   MLN4924 suppresses cilia formation by modulating AKT1. *Protein Cell.*
725   doi:10.1007/s13238-019-0614-3
726 Martinez-Cerdeno, V., Noctor, S. C., & Kriegstein, A. R. (2006). The role of intermediate progenitor
727   cells in the evolutionary expansion of the cerebral cortex. *Cereb Cortex, 16 Suppl 1*, i152-
728   161. doi:10.1093/cercor/bhk017
729 Martynoga, B., Morrison, H., Price, D. J., & Mason, J. O. (2005). Foxg1 is required for specification
730   of ventral telencephalon and region-specific regulation of dorsal telencephalic precursor
731   proliferation and apoptosis. *Dev Biol, 283*(1), 113-127.
732 Miyata, T., Kawaguchi, A., Saito, K., Kawano, M., Muto, T., & Ogawa, M. (2004). Asymmetric
733   production of surface-dividing and non-surface-dividing cortical progenitor cells.
734   *Development, 131*(13), 3133-3145. doi:10.1242/dev.01173
735 Noctor, S. C., Martinez-Cerdeno, V., Ivic, L., & Kriegstein, A. R. (2004). Cortical neurons arise in
736   symmetric and asymmetric division zones and migrate through specific phases. *Nature*
737   *neuroscience, 7*(2), 136-144. doi:10.1038/nn1172
738 Nowakowski, R. S., Lewin, S. B., & Miller, M. W. (1989). Bromodeoxyuridine immunohistochemical
739   determination of the lengths of the cell cycle and the DNA-synthetic phase for an
740   anatomically defined population. *J Neurocytol, 18*(3), 311-318.
741 Oliver, G., Sosa-Pineda, B., Geisendorf, S., Spana, E. P., Doe, C. Q., & Gruss, P. (1993). Prox 1,
742   a prospero-related homeobox gene expressed during mouse development. *Mech Dev,*
743   *44*(1), 3-16. doi:10.1016/0925-4773(93)90012-m
744 Parthasarathy, S., Srivatsa, S., Nityanandam, A., & Tarabykin, V. (2014). Ntf3 acts downstream of
745   Sip1 in cortical postmitotic neurons to control progenitor cell fate through feedback
746   signaling. *Development, 141*(17), 3324-3330. doi:10.1242/dev.114173
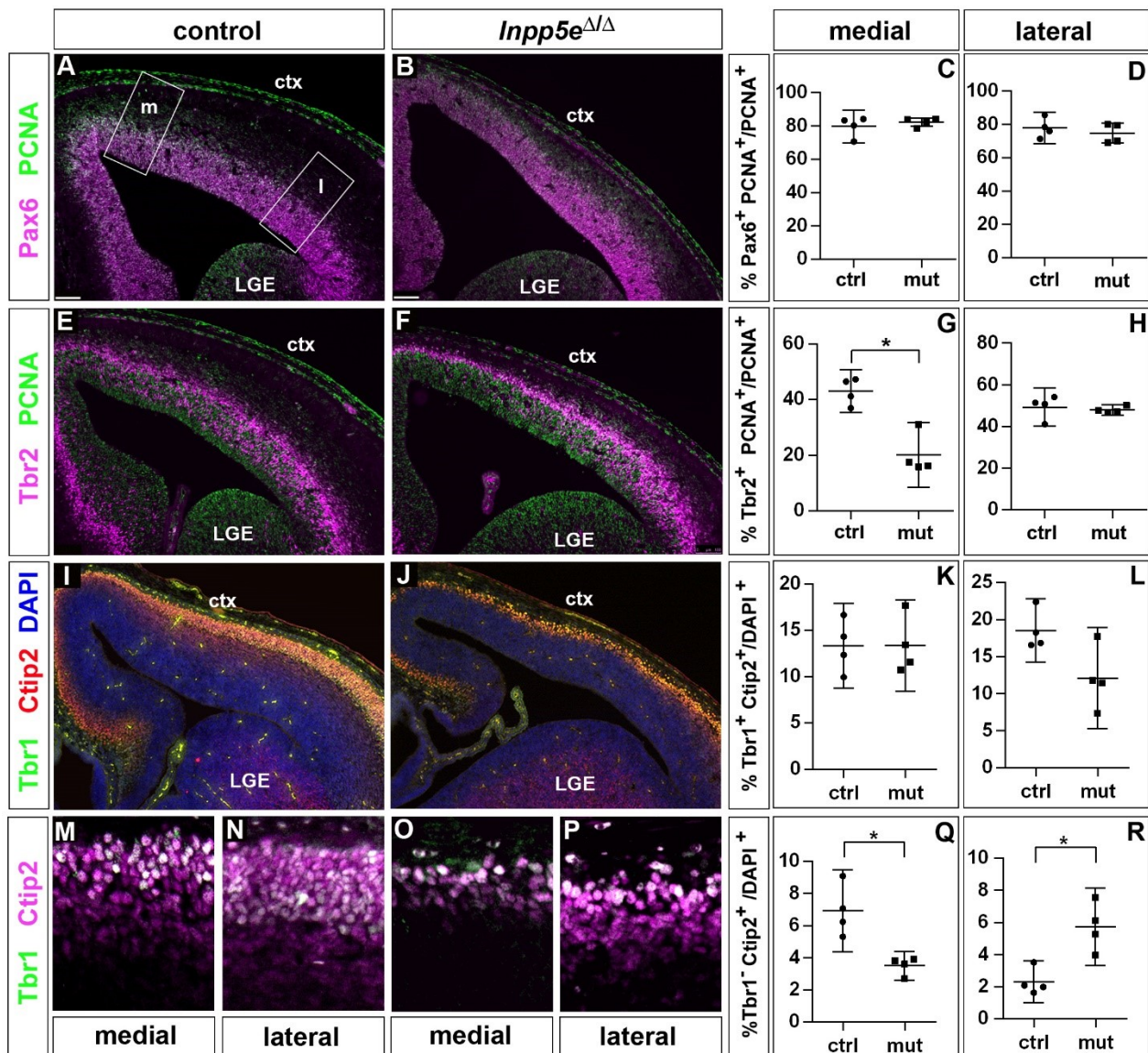
22

747 Petrova, R., Garcia, A. D., & Joyner, A. L. (2013). Titration of GLI3 repressor activity by sonic
748   hedgehog signaling is critical for maintaining multiple adult neural stem cell and astrocyte
749   functions. *The Journal of neuroscience : the official journal of the Society for Neuroscience,*
750   *33*(44), 17490-17505. doi:10.1523/JNEUROSCI.2042-13.2013
751 Plotnikova, O. V., Seo, S., Cottle, D. L., Conduit, S., Hakim, S., Dyson, J. M., . . . Smyth, I. M.
752   (2015). INPP5E interacts with AURKA, linking phosphoinositide signaling to primary cilium
753   stability. *J Cell Sci, 128*(2), 364-372. doi:10.1242/jcs.161323
754 Poretti, A., Huisman, T. A., Scheer, I., & Boltshauser, E. (2011). Joubert syndrome and related
755   disorders: spectrum of neuroimaging findings in 75 patients. *AJNR Am J Neuroradiol,*
756   *32*(8), 1459-1463. doi:10.3174/ajnr.A2517
757 Postel, M., Karam, A., Pezeron, G., Schneider-Maunoury, S., & Clement, F. (2019). A multiscale
758   mathematical model of cell dynamics during neurogenesis in the mouse cerebral cortex.
759   *BMC Bioinformatics, 20*(1), 470. doi:10.1186/s12859-019-3018-8
760 Postiglione, M. P., Juschke, C., Xie, Y., Haas, G. A., Charalambous, C., & Knoblich, J. A. (2011).
761   Mouse inscuteable induces apical-basal spindle orientation to facilitate intermediate
762   progenitor generation in the developing neocortex. *Neuron, 72*(2), 269-284.
763   doi:10.1016/j.neuron.2011.09.022
764 Putoux, A., Baas, D., Paschaki, M., Morle, L., Maire, C., Attie-Bitach, T., . . . Durand, B. (2019).
765   Altered GLI3 and FGF8 signaling underlies acrocallosal syndrome phenotypes in Kif7
766   depleted mice. *Hum Mol Genet, 28*(6), 877-887. doi:10.1093/hmg/ddy392
767 Rallu, M., Machold, R., Gaiano, N., Corbin, J. G., McMahon, A. P., & Fishell, G. (2002).
768   Dorsoventral patterning is established in the telencephalon of mutants lacking both Gli3
769   and Hedgehog signaling. *Development, 129*(21), 4963-4974.
770 Rash, B. G., & Grove, E. A. (2007). Patterning the dorsal telencephalon: a role for sonic
771   hedgehog? *J Neurosci, 27*(43), 11595-11603.
772 Reiter, J. F., & Skarnes, W. C. (2006). Tectonic, a novel regulator of the Hedgehog pathway
773   required for both activation and inhibition. *Genes Dev, 20*(1), 22-27.
774   doi:10.1101/gad.1363606
775 Sang, L., Miller, J. J., Corbit, K. C., Giles, R. H., Brauer, M. J., Otto, E. A., . . . Jackson, P. K.
776   (2011). Mapping the NPHP-JBTS-MKS protein network reveals ciliopathy disease genes
777   and pathways. *Cell, 145*(4), 513-528. doi:10.1016/j.cell.2011.04.019
778 Seuntjens, E., Nityanandam, A., Miquelajauregui, A., Debruyn, J., Stryjewska, A., Goebbels, S., . .
779   . Tarabykin, V. (2009). Sip1 regulates sequential fate decisions by feedback signaling from
780   postmitotic neurons to progenitors. *Nature neuroscience, 12*(11), 1373-1380.
781   doi:10.1038/nn.2409
782 Shi, X., Garcia, G., 3rd, Van De Weghe, J. C., McGorty, R., Pazour, G. J., Doherty, D., . . . Reiter,
783   J. F. (2017). Super-resolution microscopy reveals that disruption of ciliary transition-zone
784   architecture causes Joubert syndrome. *Nat Cell Biol, 19*(10), 1178-1188.
785   doi:10.1038/ncb3599
786 Silva, C. G., Peyre, E., & Nguyen, L. (2019). Cell migration promotes dynamic cellular interactions
787   to control cerebral cortex morphogenesis. *Nat Rev Neurosci, 20*(6), 318-329.
788   doi:10.1038/s41583-019-0148-y
789 Simeone, A., Gulisano, M., Acampora, D., Stornaiuolo, A., Rambaldi, M., & Boncinelli, E. (1992).
790   Two vertebrate homeobox genes related to the Drosophila empty spiracles gene are
791   expressed in the embryonic cerebral cortex. *EMBO J, 11*(7), 2541-2550.
792 Theil, T. (2005). Gli3 is required for the specification and differentiation of preplate neurons. *Dev*
793   *Biol, 286*(2), 559-571.
794 Theil, T., Alvarez-Bolado, G., Walter, A., & Rüther, U. (1999). Gli3 is required for Emx gene
795   expression during dorsal telencephalon development. *Development, 126*(16), 3561-3571.
796 Thomas, S., Legendre, M., Saunier, S., Bessieres, B., Alby, C., Bonniere, M., . . . Attie-Bitach, T.
797   (2012). TCTN3 mutations cause Mohr-Majewski syndrome. *Am J Hum Genet, 91*(2), 372-
798   378. doi:10.1016/j.ajhg.2012.06.017
799 Uzquiano, A., Cifuentes-Diaz, C., Jabali, A., Romero, D. M., Houllier, A., Dingli, F., . . . Francis, F.
800   (2019). Mutations in the Heterotopia Gene Eml1/EML1 Severely Disrupt the Formation of
801   Primary Cilia. *Cell Rep, 28*(6), 1596-1611 e1510. doi:10.1016/j.celrep.2019.06.096
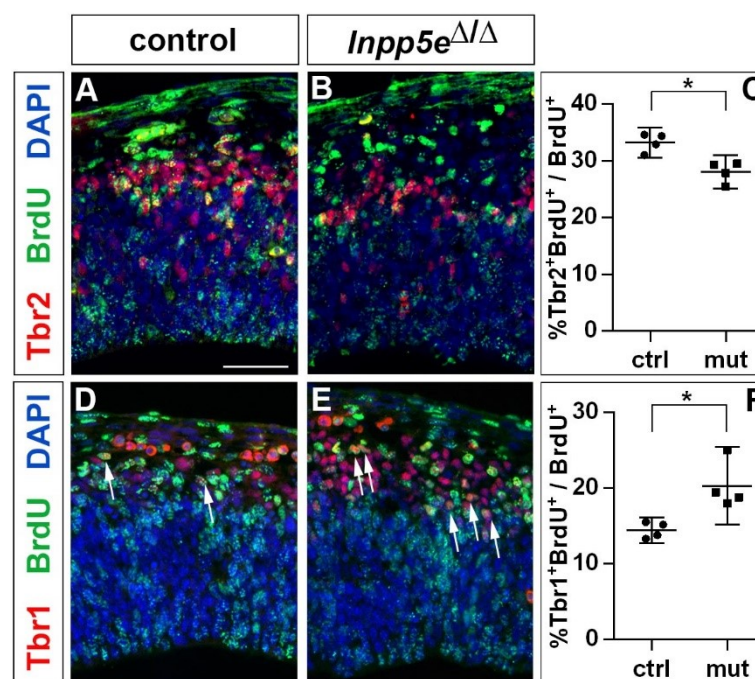
23

802 Valente, E. M., Rosti, R. O., Gibbs, E., & Gleeson, J. G. (2014). Primary cilia in
803   neurodevelopmental disorders. *Nat Rev Neurol, 10*(1), 27-36.
804   doi:10.1038/nrneurol.2013.247
805 Vasistha, N. A., Garcia-Moreno, F., Arora, S., Cheung, A. F., Arnold, S. J., Robertson, E. J., &
806   Molnar, Z. (2015). Cortical and Clonal Contribution of Tbr2 Expressing Progenitors in the
807   Developing Mouse Brain. *Cereb Cortex, 25*(10), 3290-3302. doi:10.1093/cercor/bhu125
808 Walther, C., & Gruss, P. (1991). Pax-6, a murine paired box gene, is expressed in the developing
809   CNS. *Development, 113*(4), 1435-1449.
810 Wang, C., Li, J., Meng, Q., & Wang, B. (2017). Three Tctn proteins are functionally conserved in
811   the regulation of neural tube patterning and Gli3 processing but not ciliogenesis and
812   Hedgehog signaling in the mouse. *Dev Biol, 430*(1), 156-165.
813   doi:10.1016/j.ydbio.2017.08.003
814 Wang, H., Ge, G., Uchida, Y., Luu, B., & Ahn, S. (2011). Gli3 is required for maintenance and fate
815   specification of cortical progenitors. *J Neurosci, 31*(17), 6440-6448. doi:31/17/6440 [pii]
816 10.1523/JNEUROSCI.4892-10.2011
817 Wang, H., Kane, A. W., Lee, C., & Ahn, S. (2014). Gli3 repressor controls cell fates and cell
818   adhesion for proper establishment of neurogenic niche. *Cell Rep, 8*(4), 1093-1104.
819   doi:10.1016/j.celrep.2014.07.006
820 Wang, W., Jossin, Y., Chai, G., Lien, W. H., Tissir, F., & Goffinet, A. M. (2016). Feedback
821   regulation of apical progenitor fate by immature neurons through Wnt7-Celsr3-Fzd3
822   signalling. *Nature communications, 7*, 10936. doi:10.1038/ncomms10936
823 Warren, N., Caric, D., Pratt, T., Clausen, J. A., Asavaritikrai, P., Mason, J. O., . . . Price, D. J.
824   (1999). The transcription factor, Pax6, is required for cell proliferation and differentiation in
825   the developing cerebral cortex. *Cereb Cortex, 9*(6), 627-635.
826 Wiegering, A., Petzsch, P., Kohrer, K., Ruther, U., & Gerhardt, C. (2019). GLI3 repressor but not
827   GLI3 activator is essential for mouse eye patterning and morphogenesis. *Dev Biol, 450*(2),
828   141-154. doi:10.1016/j.ydbio.2019.02.018
829 Willaredt, M. A., Hasenpusch-Theil, K., Gardner, H. A., Kitanovic, I., Hirschfeld-Warneken, V. C.,
830   Gojak, C. P., . . . Tucker, K. L. (2008). A crucial role for primary cilia in cortical
831   morphogenesis. *J Neurosci, 28*(48), 12887-12900.
832 Wilson, S. L., Wilson, J. P., Wang, C., Wang, B., & McConnell, S. K. (2012). Primary cilia and Gli3
833   activity regulate cerebral cortical size. *Dev Neurobiol, 72*(9), 1196-1212.
834   doi:10.1002/dneu.20985
835 Yee, L. E., Garcia-Gonzalo, F. R., Bowie, R. V., Li, C., Kennedy, J. K., Ashrafi, K., . . . Reiter, J. F.
836   (2015). Conserved Genetic Interactions between Ciliopathy Complexes Cooperatively
837   Support Ciliogenesis and Ciliary Signaling. *PLoS Genet, 11*(11), e1005627.
838   doi:10.1371/journal.pgen.1005627
839 Yu, J. S., & Cui, W. (2016). Proliferation, survival and metabolism: the role of PI3K/AKT/mTOR
840   signalling in pluripotency and cell fate determination. *Development, 143*(17), 3050-3060.
841   doi:10.1242/dev.137075
842 Yun, K., Potter, S., & Rubenstein, J. L. (2001). Gsh2 and Pax6 play complementary roles in
843   dorsoventral patterning of the mammalian telencephalon. *Development, 128*(2), 193-205.
844 Zhang, Y., Liu, G., Guo, T., Liang, X. G., Du, H., Yang, L., . . . Chen, B. (2020). Cortical Neural
845   Stem Cell Lineage Progression Is Regulated by Extrinsic Signaling Molecule Sonic
846   Hedgehog. *Cell Rep, 30*(13), 4490-4504 e4494. doi:10.1016/j.celrep.2020.03.027
847
848

849 **FIGURES**

Figure 1: Increased neuron formation in the dorsolateral telencephalon of E12.5 _Inpp5_$^{\Delta/\Delta}$ mutant embryos. (A-D) Pax6/PCNA double immunofluorescence staining revealed the proportion of apical radial glial cells which remained unaltered in the mutant. The boxes in (A) indicate the regions in the medial (m) and lateral (l) telencephalon at which cell counts were performed. (E-H) Reduced proportions of basal progenitors in the lateral telencephalon as revealed by staining for Tbr2 and PCNA. (I-L) Tbr1 immunostaining showed that the proportion of neurons is increased in the lateral telencephalon. All statistical data are presented as means ± 95% confidence intervals (CI); Mann Whitney tests; n = 4 except for (H) with n=5; * p < 0.05. Scale bar: 100μm. ctx: cortex; LGE: lateral ganglionic eminence.

Figure 2: Proportions of radial glial cells, basal progenitors and neurons in the neocortex of E14.5 *Inpp5e*$^{\Delta/\Delta}$ embryos. (A-D) The proportion of radial glial cells remains unaffected by the *Inpp5e* mutation as revealed by Pax6/PCNA double immunofluorescence. The boxes in A indicate the regions in the medial (m) and lateral (l) telencephalon at which cell counts were performed. (E-H) Tbr2/PCNA double staining showed a reduced proportion of basal progenitors in the *Inpp5e*$^{\Delta/\Delta}$ medial but not lateral neocortex. (I-R) Neuron formation in the *Inpp5e*$^{\Delta/\Delta}$ mutant necocortex. The proportion of Tbr1$^+$Ctip2$^+$ neurons is not significantly altered (I-L) whereas the proportion of Tbr1$^-$Ctip2$^+$ neurons is decreased and increased in the medial and lateral neocortex, respectively (M-R). All statistical data are presented as means ± 95% confidence intervals (CI); Mann Whitney tests; n = 4; * p < 0.05. Scale bars: 100µm (A) and 50µm (M). ctx: cortex; LGE: lateral ganglionic eminence.

26

874

Figure 3: Increased neurogenesis at the expense of basal progenitor formation in E12.5
***Inpp5e*$^{\Delta/\Delta}$ mutants.** Immunohistochemistry on sections of E12.5 control (A, D) and *Inpp5e*$^{\Delta/\Delta}$
embryos (B, E) that were treated with BrdU 24 hours earlier. (A-C) Tbr2/BrdU double labelling
showed that less basal progenitors formed from the BrdU labelled progenitor cohort. (D-F) The
proportion of newly formed Tbr1$^+$ neurons is increased. The arrows in D and E label Tbr1$^+$BrdU$^+$
cells. All statistical data are presented as means ± 95% confidence intervals (CI); Mann Whitney
tests; n = 4; * p < 0.05. Scale bar: 50μm.

882

883

884 **Figure 4: Increased formation of layer V neurons in E18.5 _Inpp5e_$^{\Delta/\Delta}$ mutants**. (A-F) Coronal

885 sections immunostained for the deep layer markers Tbr1 (layer VI) and Ctip2 (layer V) and for the

886 upper layer marker Satb2 (layers II-IV); there is no obvious defect in layering in the _Inpp5e_$^{\Delta/\Delta}$ mutant

887 except for the formation of a heterotopia (asterisk in D). At caudal levels, the cortex becomes thinner

888 and the rhinal fissure is shifted medially as indicated by the arrows. (G-O) Formation of cortical

889 neurons at rostrolateral levels. The proportion of Tbr1+layer VI neurons is decreased with a

890 concomitant increase in Ctip2+layer V neurons. (P-X) Portion of cortical neurons at rostromedial

891 levels. Immunolabeling with cortical layer markers revealed no significant difference. Note that due

892 to the thinner cortex, the position of layer VI Tbr1+ (Q) and layer V Ctip2+ neurons (J, S) appears to

893 be shifted to more superficial positions, however, the relative order of these layers remains

894 unaffected. All statistical data are presented as means ± 95% confidence intervals (CI); Mann

895 Whitney tests; n = 4; * $p < 0.05$. Scale bars: 500μm (A) and 100μm (G). CC: corpus callosum; ctx:

896 cortex; sep: septum; str: striatum.

897
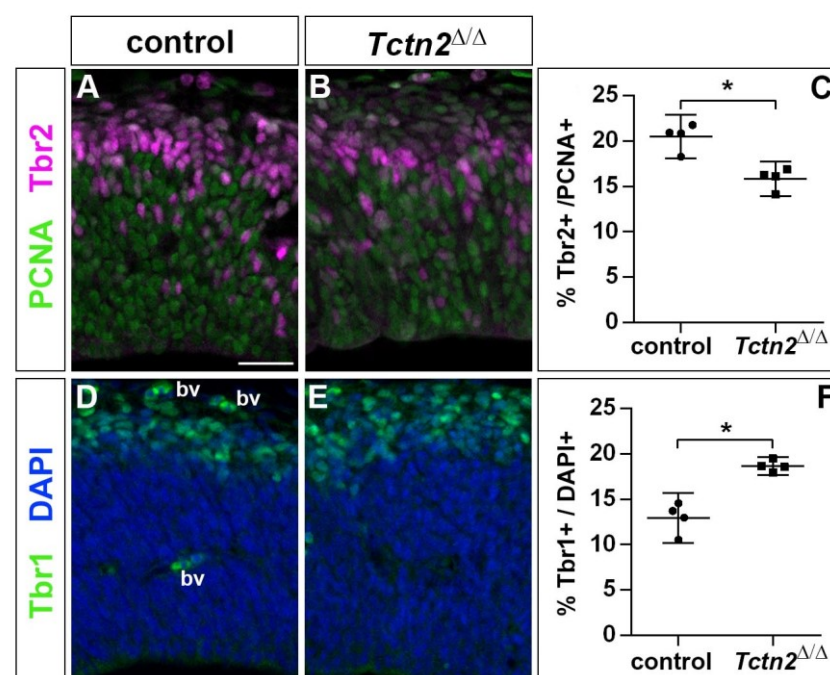
Figure 5: Increased generation of cortical neurons in E12.5 *Tctn2*^{-/-} embryos. (A-C) Double immunofluorescence for PCNA and Tbr2 revealed a significantly decreased proportion of basal progenitors. (D-F) The portion of Tbr1^{+} cortical neurons is increased. All statistical data are presented as means ± 95% confidence intervals (CI); Mann Whitney tests; n = 4; * p < 0.05. Scale bar: 50μm. bv: blood vessel.

905
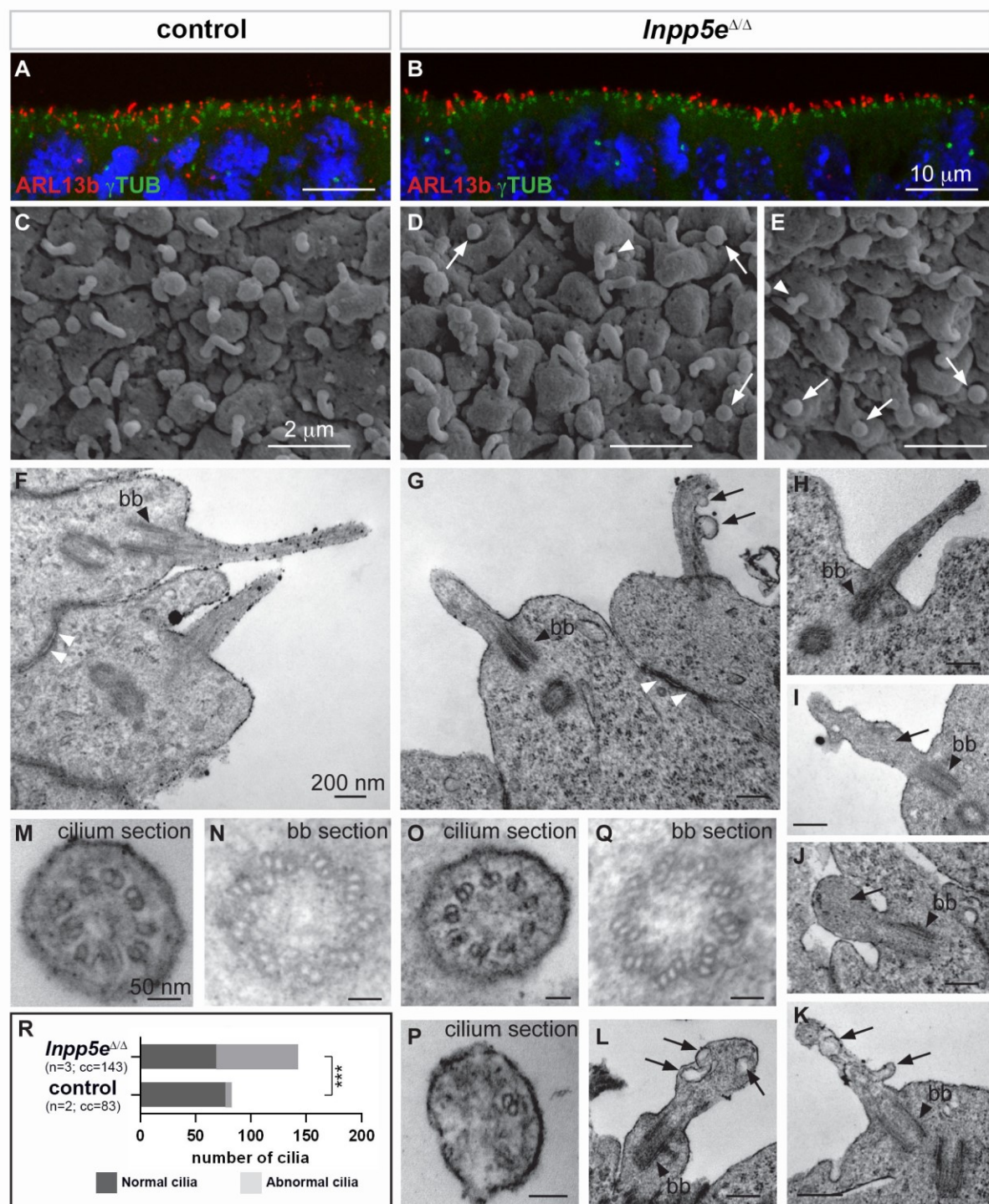
Figure 6: Ciliary defects in E12.5 *Inpp5e*$^{\Delta/\Delta}$ forebrain. (A-B) Immunohistochemistry for Arl13b and γ-Tubulin (γTUB) on E12.5 brain cryosections showed an accumulation of ciliary axonemes and basal bodies, respectively, at the apical border of radial glial cells facing the ventricules in both control (A) and *Inpp5e*$^{\Delta/\Delta}$ (B) embryos without any obvious difference. Scale bars: 10 μm.

(C-E) Scanning electron microscopy (SEM) on E12.5 control (C) and *Inpp5e*$^{\Delta/\Delta}$ (D, E) brains highlighted the presence of primary cilia projecting from the apical surface of radial glial cells in both control (A) and *Inpp5e*$^{\Delta/\Delta}$ (B) embryos. However, SEM also revealed the presence of abnormal cilia

31

913 in *Inpp5e*$^{\Delta/\Delta}$ embryos having a spherical shape (arrows in D and E) or aberrant lateral buddings

914 (arrowheads in D and E). Scale bars: 2 μm.

915 (F-L) Transmission electron microscopy (TEM) analysis on E12.5 brains showed longitudinal

916 sections of primary cilia in control (F) and *Inpp5e*$^{\Delta/\Delta}$ (G-L) embryos. In control primary cilia, the

917 axoneme appeared as an extension of the basal body (bb, black arrowheards) (F-H). In addition to

918 cilia with normal morphology, abnormal cilia were identified in *Inpp5e*$^{\Delta/\Delta}$ embryos thanks to the

919 presence of a basal body apparently correctly docked to the apical membrane. Abnormal cilia lacked

920 an axoneme (I, J, L) or showed unusual membranous structures, such as budding (G, K) or internal

921 (I, K, L) vesicles (arrows) or undulating peripheral membranes (I). Note that tight junctions (white

922 arrowheads in F and G) appeared normal in *Inpp5e*$^{\Delta/\Delta}$ (G) and control (F) embryos, suggesting that

923 apico-basal polarity of *Inpp5e*$^{\Delta/\Delta}$ radial glial cells was not compromised. Scale bars: 200 nm.

924 (M-Q) TEM images showing transverse sections of the axoneme (M, O, P) and the basal body (N,

925 Q) in control (M, N) and *Inpp5e*$^{\Delta/\Delta}$ (O-Q) embryos with no major difference in the basal bodies

926 between control (N) and *Inpp5e*$^{\Delta/\Delta}$ (Q) embryos. However, transverse section of primary cilia in

927 *Inpp5e*$^{\Delta/\Delta}$ brains revealed the presence of normal axonemes composed of 9 correctly organized

928 doublets of microtubules on some radial glial cells (O), while others harboured an abnormal axoneme

929 containing a lower number of microtubule doublets (P). Scale bars: 50 nm. (R) Graph showing the

930 number of normal versus abnormal cilia (cil.) found on TEM images from control (n=3) or *Inpp5e*$^{\Delta/\Delta}$

931 (n=3) embryos. cc: counted cilia.

932
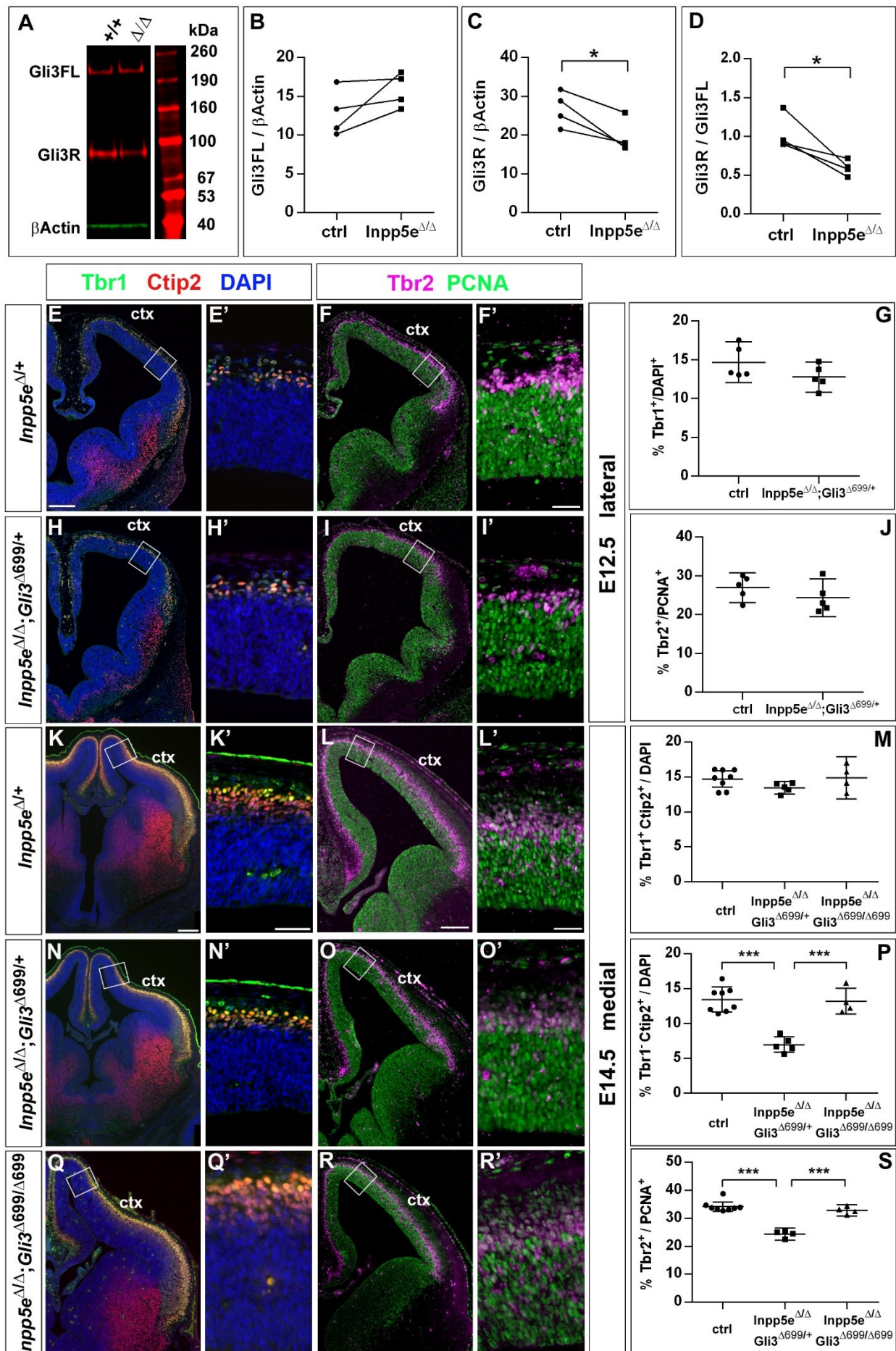
934 **Figure 7: Re-introducing the Gli3 repressor rescues the neurogenesis defect in *Inpp5e***

935 ***mutants***. (A-D). Gli3 Western blot on E12.5 dorsal telencephalic tissue revealed the Gli3 full length

936 (FL) and repressor (R) forms (A). While Gli3FL levels are not affected (B), levels of Gli3R (C) and

937 the Gli3R/Gli3FL ratio (D) are decreased in *Inpp5e*$^{\Delta/\Delta}$ embryos. A paired t-test was used to evaluate

938 levels of Gli3FL and Gli3R and the Gli3R/Gli3FL ratio in four control/*Inpp5e*$^{\Delta/\Delta}$ embryo pairs derived

939 from four different litters. (E-S) Formation of basal progenitors and neurons in the neocortex of

940 *Inpp5e*$^{\Delta/\Delta}$;Gli3$^{\Delta699/+}$ and *Inpp5e*$^{\Delta/\Delta}$;Gli3$^{\Delta699/699}$ embryos. (E-N) In the lateral neocortex of E12.5

941 embryos, there is no significant difference in the proportions of Tbr1+ neurons (E-G) and basal

942 progenitor cells (H-J) between control and *Inpp5e*$^{\Delta/\Delta}$;Gli3$^{\Delta699/+}$ embryos. (K-S) In the E14.5 medial

943 neocortex, the proportion of Tbr1$^-$Ctip2$^+$ neurons (P) and basal progenitors (S) are significantly

944 reduced in *Inpp5e*$^{\Delta/\Delta}$;*Gli3*$^{\Delta699/+}$ embryos but not in *Inpp5e*$^{\Delta/\Delta}$;Gli3$^{\Delta699/699}$ embryos. All statistical data

945 except for the Western blot data (C, D) are presented as means ± 95% confidence intervals (CI);

946 Mann Whitney (n=5) (G, J) and ONE way ANOVA followed by Tukey's multiple comparison test (J,

947 M, P); * $p < 0.05$; ** $p < 0.01$; *** $p < 0.001$. Scale bars: 50μm (E, K, L), 100μm (A), and 250μm (F',

948 K', L'). ctx: cortex; MGE: medial ganglionic eminence; LGE: lateral ganglionic eminence.

949